



This is a repository copy of *Axions beyond gen 2*.

White Rose Research Online URL for this paper:
<https://eprints.whiterose.ac.uk/209303/>

Version: Published Version

Article:

Boutan, C. orcid.org/0000-0002-1470-1946, Carosi, G. orcid.org/0000-0003-0130-6979, Rosenberg, L.J. orcid.org/0000-0003-0686-0485 et al. (23 more authors) (2023) Axions beyond gen 2. *International Journal of Modern Physics A*, 38 (33 & 34). 2330012. ISSN 0217-751X

<https://doi.org/10.1142/s0217751x23300120>

Reuse

This article is distributed under the terms of the Creative Commons Attribution (CC BY) licence. This licence allows you to distribute, remix, tweak, and build upon the work, even commercially, as long as you credit the authors for the original work. More information and the full terms of the licence here:
<https://creativecommons.org/licenses/>

Takedown

If you consider content in White Rose Research Online to be in breach of UK law, please notify us by emailing eprints@whiterose.ac.uk including the URL of the record and the reason for the withdrawal request.



eprints@whiterose.ac.uk
<https://eprints.whiterose.ac.uk/>

 OPEN ACCESS

International Journal of Modern Physics A
Vol. 38, Nos. 33 & 34 (2023) 2330012 (63 pages)

© The Author(s)

DOI: [10.1142/S0217751X23300120](https://doi.org/10.1142/S0217751X23300120)

 **World Scientific**
www.worldscientific.com

Axions beyond Gen 2

Christian Boutan [†]

*Pacific Northwest National Laboratory,
Richland, WA 99352, USA*

Gianpaolo Carosi [†]

*Lawrence Livermore National Laboratory,
Livermore, CA 94550, USA*

Leslie J Rosenberg ^{*,†} and Gray Rybka [†]


*Department of Physics, University of Washington,
Box 351560, Seattle, WA 98195-1560, USA
ljrberg@uw.edu

K. M. Backes [‡]

*Department of Physics, Yale University,
New Haven, Connecticut 06511, USA*

Chelsea Bartram [‡]

*SLAC Linear Accelerator Center,
Menlo Park, CA 94025-7015, USA*

Masha Baryakhtar [‡]

*Department of Physics, University of Washington,
Box 351560, Seattle, WA 98195-1560, USA*

Mark D. Bird [‡]

*National High Magnetic Field Laboratory,
Tallahassee, FL 32310, USA*

Caterina Braggio [‡]

Dipartimento di Fisica e Astronomia, Padova, Italy

Dmitry Budker [‡]


*Helmholtz Institute — Johannes Gutenberg University,
Mainz, Germany and UC Berkeley, Berkeley, CA, USA*

* Corresponding author.


† Proceedings editors.

‡ Proceedings contributors.

This is an Open Access article published by World Scientific Publishing Company. It is distributed under the terms of the [Creative Commons Attribution 4.0 \(CC BY\)](https://creativecommons.org/licenses/by/4.0/) License which permits use, distribution and reproduction in any medium, provided the original work is properly cited.

Raymond T. Co [‡]


*William I. Fine Theoretical Physics Institute,
School of Physics and Astronomy,
University of Minnesota, Minneapolis, MN 55455, USA*

Edward Daw [‡]

University of Sheffield, Sheffield, UK

Akash Dixit [‡]


University of Chicago, Chicago, IL 60637, USA

Andrew A. Geraci [‡]

Northwestern University, Evanston, IL 60208, USA

Chang Lee [‡]


*Max-Planck-Institut für Physik (Heisenberg-Institut),
Fohringer Ring 6 München 80805, Germany*

Soohyung Lee [‡]


*Center for Axion and Precision Physics Research,
Institute for Basic Science (IBS/CAPP),
Daejeon 34051, Republic of Korea*

David Marsh [‡]


Kings College London, London, UK

Ciaran O'Hare [‡]

*School of Physics, The University of Sydney,
Camperdown, NSW 2006, Australia*

Ken'ichi Saikawa [‡]


*KITP Kanazawa University,
Kakuma-Machi, Kanazawa 920-1192, Japan*

Chiara P. Salemi [‡]

*Laboratory for Nuclear Science,
Massachusetts Institute of Technology Cambridge, MA 02139, USA*

Yannis K. Semertzidis [‡]


*Center for Axion and Precision Physics Research,
Institute for Basic Science (IBS/CAPP),
Daejeon 34051, Republic of Korea*

Andrew Sonnenschein [‡]

*Fermi National Accelerator Laboratory,
Batavia, IL 60510, USA*

Aaron Spector [‡]


DESY, Hamburg, Germany

Michael E. Tobar 

*ARC Centre of Excellence for Engineered Quantum Systems
and ARC Centre of Excellence for Dark Matter Particle Physics,
Department of Physics, University of Western Australia,
35 Stirling Highway, Crawley, WA 6009, Australia*

Julia Vogel 

*Lawrence Livermore National Laboratory,
Livermore, CA 94550, USA*

Ariel Zhitnitsky 

*University of British Columbia,
Dept. of Physics, Vancouver, BC, Canada*

Received 25 May 2023

Accepted 10 August 2023

Published 23 January 2024

The QCD (Quantum ChromoDynamics) axion emerged as one of the best-motivated dark matter candidates. In 2018, the Axion Dark Matter eXperiment (ADMX), one of the U.S. Department of Energy’s “Gen 2” flagship dark-matter projects, demonstrated first sensitivity to the highly plausible “DFSZ” dark matter axion couplings over a small frequency range. We anticipate this development marks the first step in constructing yet more powerful experiments that can explore large swaths of the axion parameter space at high sensitivity and result in a discovery. But, realizing this requires advances in both our understanding of the theory and experiment design. Between 25 January and 27 January 2021, the “Axions Beyond Gen 2 Workshop” was held, where selected members of the community discussed our broad understanding of the QCD axion and charted a course for future experiments having sensitivity and mass reach well beyond the current “Gen 2” experiments. These proceedings are summaries of the topics presented and discussed.

Keywords: Axions; QCD axions; axion production; axion cosmology; dark matter; axion detectors

Content

1. Introduction	4
2. Axion Theory	5
2.1. New roles of the QCD axion in dark matter and baryogenesis (Raymond T. Co)	6
2.2. Production of axions in the early universe (Ken’ichi Saikawa)	7
2.3. Axion Quark Nuggets and Matter–Antimatter Asymmetry as Two Sides of the Same Coin: Theory, Observations and Future Experimental Searches (Ariel Zhitnitsky)	10
2.3.1. Axion quark nuggets (AQN) model basics	10
2.3.2. Broadband axion searches and the daily modulations	10
3. Cosmology and Astrophysics	11
3.1. Dark matter in the milky way and implications for axion searches (Ciaran O’Hare)	11

3.2.	Black holes and axions: From gravitational waves to axionic beacons (Masha Baryakhtar)	14
4.	Current Dark Matter Axion Searches	16
4.1.	Probing the axion–electron and axion–photon couplings with the QUAX haloscopes (Caterina Braggio)	17
4.2.	Wavelike dark matter on the horizon: Searching for the DFSZ axion with the ADMX haloscope (Chelsea Bartram)	19
4.3.	Lumped-Element searches for low-mass axion dark matter (Chiara P. Salemi)	20
4.4.	Axion search activities at IBS/CAPP (Soohyung Lee)	22
4.5.	Axion program at the university of western Australia (Michael E. Tobar)	23
4.5.1.	ORGAN	23
4.5.2.	UPLOAD	24
4.5.3.	BEAST	24
4.6.	Post-inflationary axion dark matter search with a dielectric haloscope (Chang Lee)	25
4.7.	What is up, CASPER? (Dmitry Budker for the CASPER Collabo- ration)	27
5.	Non-Dark-Matter Axion Searches	29
5.1.	The status of solar axion searches and the international axion ob- servatory (IAXO) (Julia Vogel)	29
5.2.	ALPS II (Aaron Spector)	31
5.3.	Searching for the QCD axion with ARIADNE (Andrew A. Geraci)	34
6.	New Ideas and New Technologies	35
6.1.	Broadband axion searches with coaxial dish antennas (Andrew Sonnenschein)	37
6.2.	Axion quasiparticles for axion dark matter detection (David Marsh)	39
6.3.	Searching for dark matter with a superconducting qubit (Akash Dixit)	41
6.4.	Resonant feedback (Ed Daw)	42
6.5.	High-temperature superconductor magnets for axion dark matter searches (Yannis K. Semertzidis)	45
6.6.	An overview of high field HTS solenoid technology (Mark D. Bird)	46
6.7.	Enhancing axion detection with quantum squeezing (K. M. Backes for the HAYSTAC collaboration)	47
7.	Conclusion	50

1. Introduction

The QCD (Quantum ChromoDynamics) axion emerged as one of the best-motivated dark matter candidates. In 2018, the Axion Dark Matter eXperiment (ADMX), one of

the U.S. Department of Energy’s “Gen 2” flagship dark matter projects, demonstrated first sensitivity to the highly plausible “DFSZ” dark matter axion couplings over a small frequency range. We anticipate this development marks the first step in constructing yet more powerful experiments that can explore large swaths of the axion parameter space at high sensitivity and result in a discovery. But, realizing this requires advances in both our understanding of the theory and experiment design.

Between 25 January and 27 January 2021, the “Axions Beyond Gen 2 Workshop” was held, where selected members of the community discussed our broad understanding of the QCD axion and charted a course for future experiments having sensitivity and mass reach well beyond the current “Gen 2” experiments. These proceedings are summaries of the topics presented and discussed. The topics are arranged with the following questions in mind:

- **Axion Theory** What theories underlie the standard QCD axion? What are the preferred masses and couplings for experiments to target?
- **Cosmology and Astrophysics** What is the distribution of axion dark matter near our location in the galaxy? What astrophysical measurements influence terrestrial experiment design?
- **Current Dark Matter Axion Searches** What is the progress made by the current generation “Gen 2” style experiments?
- **Non-Dark Matter Axion Searches** What are the prospects for axion searches that do not depend on axions being the local dark matter for influencing dark matter experiments?
- **New Ideas and Developing Technologies** What are the critical technologies to enable future axion dark matter searches? What advancements could fundamentally change the design of future experiments?

The limitations of time and space, as well as the considerable challenges related to holding an online workshop during the COVID-19 pandemic, would not allow complete answers to any of these questions. However, the presentations and discussions summarized in the following sections show that significant progress has been made and there are paths to a future discovery.

2. Axion Theory

The standard QCD (or PQWW — Peccei–Quinn–Weinberg–Wilczek) axion is expected to be largely produced nonthermally in the early universe through the “misalignment mechanism”, with very approximate axion masses around $1 \mu\text{eV}$. Axions with these masses yield the density of dark matter observed today. At this workshop, we discussed a number of extensions to this cosmological model, with particular focus on tying the axion production mechanism to the observed matter–antimatter asymmetry in the universe. Additional production mechanisms were proposed that could push the axion dark matter mass higher (or lower), though

considerable phenomenological uncertainty remains and it is uncertain whether axions with masses considerably higher or lower than the original PQWW axion can be a dominant component of dark matter.

2.1. *New roles of the QCD axion in dark matter and baryogenesis (Raymond T. Co)*

We propose a paradigm where the QCD axion's unexplored cosmological evolution, a rotation in the field space, gives rise to the observed dark matter and baryon asymmetry of the Universe.

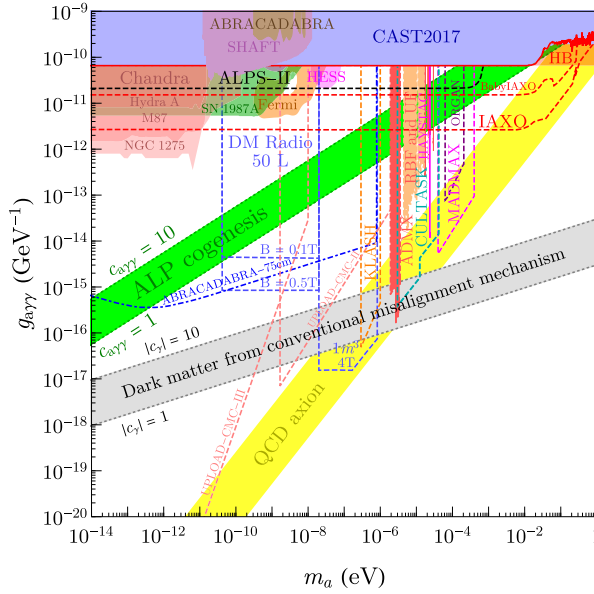
The rotation is initiated by explicit Peccei–Quinn (PQ) symmetry breaking effective in the early Universe. Such explicit PQ breaking from higher dimension operators is expected because it is believed that quantum gravity does not respect global symmetries. This effect is typically negligible in the present day because of the large separation between the decay constant and the cutoff scale of the theory. However, in the early Universe, the value of the PQ breaking field, which is the decay constant, can be as large as the cutoff scale of the theory, e.g. due to its interaction with the inflaton physics. In this case, a rotation is initiated by the axion mass from explicit PQ breaking at the onset of the motion.

The axion rotation can lead to a larger axion abundance, via the kinetic misalignment mechanism,^{1,2} than from the conventional misalignment mechanism.^{3–5} As long as the axion field velocity is much larger than its mass $\dot{\theta} \gg m_a$, the axion continues to run over the potential barriers. For a sufficiently fast rotation, this motion continues past the time when the mass is equal to Hubble, then the axion kinetic energy $\dot{\theta}^2 f_a^2$ is much larger than the maximum possible potential energy $\theta_i^2 m_a^2 f_a^2$ in the conventional case, and thus the abundance is enhanced.

The observed cosmological excess of matter over antimatter can also originate from the axion rotation. The $U(1)$ charge associated with the rotation is transferred to the baryon asymmetry via the Standard Model sphaleron processes and other processes that violate $B - L$.

A correlated prediction of the axion mass and coupling strength can be made from the rotation necessary to produce the observed abundances of axion dark matter via kinetic misalignment and of the baryon asymmetry via mechanisms discussed below.

Due to the presence of the strong anomaly for the QCD axion, the strong sphaleron processes transfer the rotation into the quark chiral asymmetry, which is then reprocessed into the baryon asymmetry via the electroweak sphaleron processes. Such a scenario, called axiogenesis,⁷ predicts the QCD axion with a mass around $\mathcal{O}(0.1 - 100)$ meV, i.e. toward the upper end of the yellow bands in Figs. 1 and 2. If the QCD axion or ALP has an electroweak anomaly, then the rotation can directly produce the baryon asymmetry by the electroweak sphaleron processes.⁶ The scenario for ALPs is called ALP-cogenesis and predicts the axion coupling to be in the green bands in Figs. 1 and 2.



Source: From Ref. 6.

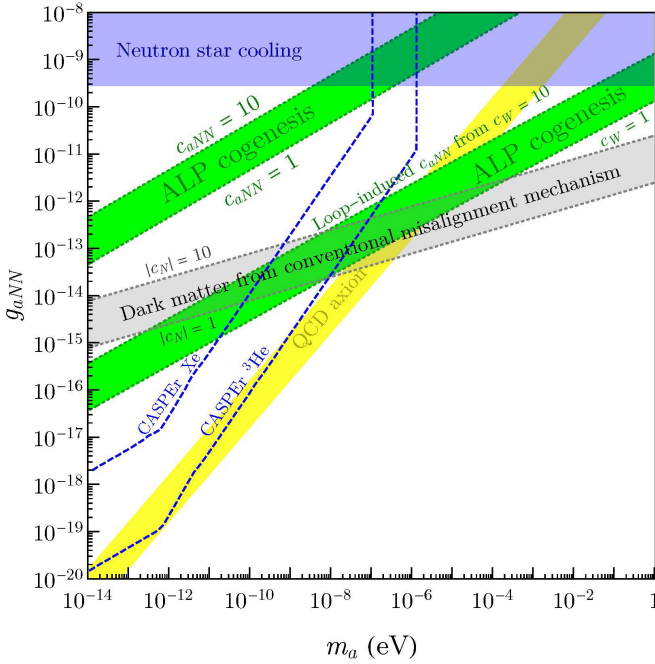
Fig. 1. (Color online) The prediction for the axion-like particle (ALP)-photon coupling is shown by the green band in the left panel. The predictions for the QCD axion and for ALP dark matter from the conventional misalignment mechanism are shown in the yellow and gray bands. Other shaded regions denote the existing experimental constraints, while various lines show the sensitivity of future experiments.

In the presence of a neutrino Majorana mass term, which violates the lepton number, the transfer of the asymmetries can be more efficient. In this scenario, named lepto-axiogenesis,⁸ when a lepton number is created at high temperatures, a nonzero $B - L$ number is created, which is preserved by the electroweak sphaleron processes. Since the production of $B - L$ at high temperatures depends on whether the lepton number violating interactions are in equilibrium, the determination of the final baryon number is sensitive to the full cosmological evolution. Ultimately, in the concrete models considered in lepto-axiogenesis,⁸ the QCD axion is predicted to lie within a similar mass and coupling range as that in axiogenesis. Despite the similar predictions in axion parameter space, lepto-axiogenesis and axiogenesis make other qualitatively different predictions, such as the electroweak phase transition temperature and the mass of the PQ breaking field.

In summary, we have presented a novel possibility for the QCD axion and the ALPs to simultaneously solve multiple open questions in particle physics. Most excitingly, this paradigm makes predictions for the axions that are within the reach of current and planned experiments.

2.2. Production of axions in the early universe (Ken'ichi Saikawa)

The axion produced via nonthermal processes in the early Universe is regarded as a strong candidate for cold dark matter (CDM).^{3,5,9} Since its relic abundance depends



Source: From Ref. 6.

Fig. 2. (Color online) The prediction for the axion-like particle ALP-nucleon coupling is shown by the green band in the right panel. The predictions for the QCD axion and for ALP dark matter from the conventional misalignment mechanism are shown in the yellow and gray bands. Other shaded regions denote the existing experimental constraints, while various lines show the sensitivity of future experiments.

on the unknown parameter, the axion decay constant or axion mass, the estimation of the relic abundance can be used to predict the value of axion mass that can account for CDM. In order to obtain a precise theoretical estimate of the axion dark matter mass, it is thus crucial to understand its production mechanisms.

A well-known mechanism is the so-called misalignment mechanism,^{3,5,9} which can be straightforwardly applied to the case where the PQ symmetry has been broken before inflation and is never restored. On the other hand, if the PQ symmetry has been restored and broken after inflation, topological defects (strings and domain walls) are formed, and could have an important role in the calculation of the axion relic abundance.¹⁰ In this post-inflationary PQ symmetry breaking scenario, the axion mass prediction can also depend on the number N_{DW} of CP-conserving minima after the QCD phase transition, and hence on the ultraviolet completion of the axion model: If $N_{\text{DW}} = 1$, the network of string-wall systems decays soon after the QCD phase transition, leading to a prediction for the axion dark matter mass of $\mathcal{O}(10 - 100) \mu\text{eV}$. The case with $N_{\text{DW}} > 1$ is basically excluded since the string-wall network is stable, but there is a possibility to avoid the problem if there exists a small energy bias that breaks the degeneracy of vacua. In that case, the axion could

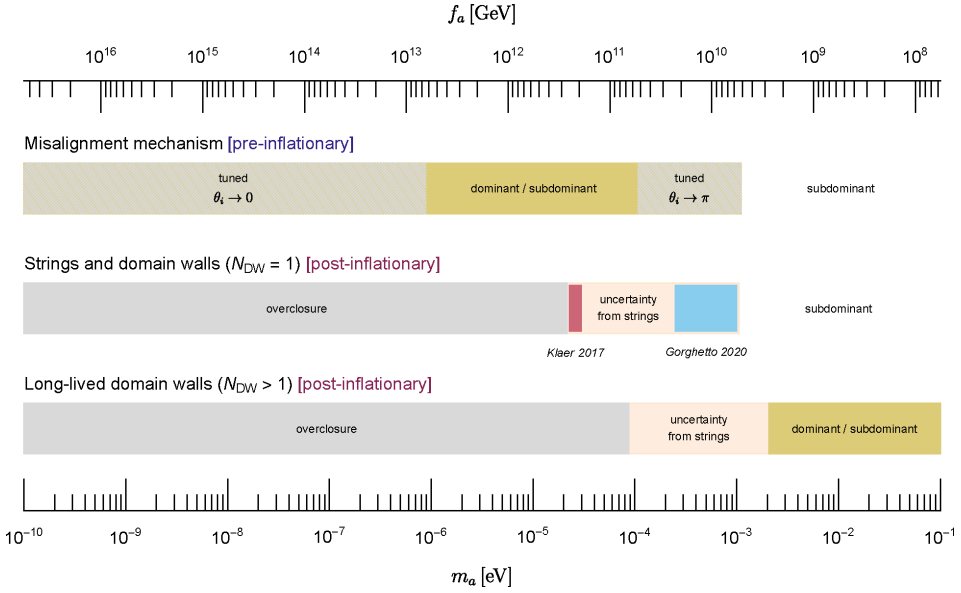


Fig. 3. Axion dark matter mass range. Courtesy of Ken'ichi Saikawa.

account for CDM at higher mass ranges.¹¹ The axion dark matter mass ranges predicted by various different early universe scenarios are summarized in Fig. 3.

Recently, several groups have been working on simulations of axion production in the post-inflationary scenario to obtain a more reliable estimate of the axion abundance from strings. The fundamental challenge is that one cannot simulate the physically relevant regime of axion strings due to the fact that the string tension acquires a large logarithmic correction, which is associated with a huge hierarchy between the PQ scale and axion mass at the QCD epoch. One possible approach is to calculate the axion production efficiency at the large-log regime directly by using an effective description, the result of which points to the axion dark matter mass of $26.2 \pm 3.4 \mu\text{eV}$.¹² However, this result was challenged by another approach relying on an extrapolation from the scaling solution,¹³ which found that the axion production could be more efficient than the standard misalignment calculation. The latter approach predicts a higher mass of $\sim 500 \mu\text{eV}$,¹³ which is strongly discrepant with the former one.^a

The above discrepancy should be attributed to our limited knowledge of the spectrum of axions around the QCD epoch, and a more careful study of the low momentum axion distribution with improved dynamical ranges would be highly motivated. The ongoing large-scale simulations comprise up to $10,000^3$ lattice points,¹⁵ which enable us to reach the value of the logarithmic parameter $\log \lesssim 8.5$.

^aMore recently, a new large scale simulation was performed based on the adaptive mesh refinement method.¹⁴ The extrapolation of its outcome leads to a mass prediction of $40 - 180 \mu\text{eV}$, which is discrepant with the results of Refs. 12 and 13.

This value is still far from the realistic value ($\log \sim 70$), but very close to the critical point, $\log \sim 9 - 10$ suggested by Ref. 13, where the axion spectrum would change its shape from the ultraviolet-dominated to the infrared-dominated form, for which the axion field distribution could be nonlinear. Hence it would be interesting to investigate the behavior of axion strings around this critical point on near-future supercomputers. Confirming or excluding such a possibility of the nonlinear regime by use of direct numerical simulations should considerably improve our understanding of the axion production efficiency and reduce the uncertainty in axion dark matter mass prediction.

2.3. Axion quark nuggets and matter–antimatter asymmetry as two sides of the same coin: Theory, observations and future experimental searches (Ariel Zhitnitsky)

2.3.1. Axion quark nuggets (AQN) model basics

The matter–antimatter asymmetry and dark matter are known to be the two most challenging problems of the modern cosmology. It is commonly assumed that there are two stories here. The first is called the baryogenesis, which explains the matter–antimatter asymmetry in the Universe. The second is the presence of dark matter in our Universe. It has been advocated in Ref. 16, that these two fundamental problems could be two sides of the same coin in which case the dark matter density Ω_{DM} and the baryonic matter density Ω_{visible} will automatically assume the same order of magnitude $\Omega_{\text{DM}} \sim \Omega_{\text{visible}}$ without any fine tuning, and irrespective to any specific details of the model, such as the axion mass m_a . This is because both components are proportional to the same fundamental Λ_{QCD} scale, and both components are formed during the same QCD transition, see recent review in Ref. 17 for details.

There are several additional elements in the AQN model in comparison with previous constructions. First, there is an additional stabilization factor provided by the axion domain walls, which are copiously produced during the QCD transition. Another crucial additional element of the AQN proposal is that the nuggets could be made of *matter* as well as *antimatter* during the QCD epoch. Both new elements play an important role in the axion search experiments to be discussed below.

2.3.2. Broadband axion searches and the daily modulations

This goal is to highlight the basic ideas developed in Refs. 18 and 19 on possible strategies to search for the AQN-induced axions. The most important feature of the AQN-induced axions is that they will be released with relativistic velocities with average value $\langle v_{\text{axion}}^{\text{AQN}} \rangle \simeq 0.6c$. This feature should be contrasted with conventional galactic nonrelativistic axions $v_{\text{axion}} \sim 10^{-3}c$. The large velocities of the emitted axions by AQNs dramatically changes the entire strategy of axion searches. This is because the axions are characterized by broadband distribution with $m_a \lesssim \omega_a \lesssim 1.8m_a$. Therefore, the corresponding axion detectors must be some kind of broadband instruments.

A novel element that may dramatically increase discovery potential is the presence of daily modulations (unique for AQN model) when the AQN-induced axion density varies with time during the day:

$$\rho_a^{\text{AQN}}(t) \equiv \langle \rho_a^{\text{AQN}}(R_{\oplus}) \rangle [1 + \kappa_{(d)} \cos(\Omega_d t - \phi_0)], \quad (1)$$

where ϕ_0 is the phase shift, which can be assumed to be constant on the scale of a season. However, it actually slowly changes during a year due to the variation of the direction of dark matter wind with respect to the Earth.

Therefore, the idea is to collect the signal for each hour of the day during the same season of the year in broad frequency band $\Delta\omega \in (1 - 1.8)m_a$, and fit to the modulation formula (1) to extract parameter $\kappa_{(d)}$. The recording of the daily modulations in terms of $\kappa_{(d)} \approx (10 - 20)\%$ would be a very strong support for the AQN model as any weakly interacting massive particle models predict negligible effect on a level of $\lesssim 0.1\%$. One should also add that any axion search instruments presently operating can, in principle, analyze the daily modulations along the lines described above. This obviously may include all previously collected data sets. In particular, the CAST-CAPP collaboration is presently analyzing their existing data from all cavities to search for possible daily modulations. There are a number of consistency checks that dramatically diminish the spurious signals. First, the modulation ($\kappa_{(d)} \neq 0$) must manifest itself in a single frequency band, and must not be present in other frequency bands. The modulation must also be absent at zero field. One more consistency check is the study of the phase ϕ_0 , which must demonstrate the drift with a season during a year.

3. Cosmology and Astrophysics

The existence of axions would affect a number of astrophysical processes: for instance stellar evolution, cooling of neutron stars, and the neutrino flux from supernova. Lack of these observed signatures provide stringent limits for axion couplings and masses, independent of whether axions are a primary component of dark matter. At the workshop, a relatively new axion-related astrophysical observable was discussed: the effect of axions on black hole spin and gravitational waves; this observable can constrain low-mass axions with surprising sensitivity.

Another outstanding issue discussed at the workshop was how to relate our global theories of axion production cosmologically to the local phase-space structure of axions near Earth given the large amount of new information from recent galactic surveys. There is also the long-standing question of whether axion dark matter is smoothly distributed or is clumped into subhalos. These are important questions for predicting signals of interest in terrestrial detectors.

3.1. *Dark matter in the milky way and implications for axion searches (Ciaran O’Hare)*

All experiments seeking to directly detect axions in the vicinity of the Earth are confronted by an unavoidable astrophysical uncertainty. The two main quantities

that we need when predicting signals are (1) the dark matter density ρ_{DM} and (2) the velocity distribution $f(v)$. Assuming we make some measurement of the axion field over many coherence times ($T \gtrsim 10^6 m_a^{-1}$), we can write a generic relationship between these astrophysical quantities and some power spectrum extracted from the field oscillations

$$P(\omega) \propto \alpha \rho_{\text{DM}} f(\omega), \tag{2}$$

where the unwritten constants of proportionality will depend on the specifics of the experiment.

We have written the lab-frame dark matter speed distribution as a function of the axion frequency by changing variables to $\omega = m_a(1 + v^2/2)$. The constant α is an exponentially distributed number that arises from the stochastic variations in the Fourier amplitudes of the axion field and contribute to the measured power at a given frequency.²⁰ Assuming there are no phase correlations between Fourier modes, then at every value of ω in the discrete Fourier transform of some time-series data, a different value of α is drawn. For experiments that measure the field over times that are long compared to the coherence time, this stochasticity can be suppressed by stacking power spectra together. However, if the coherence time is very long, then these random amplitudes can significantly impact the expected signal statistics.²¹

The baseline assumption for the Milky Way’s dark matter halo is the Standard Halo Model (SHM), which results in a Maxwellian form for $f(v)$ (shown as $\alpha f(\omega)$, in Fig. 4). The SHM is isotropic in the galactic rest frame, but we observe $f(v)$ after a boost into the experiment’s rest frame by the velocity of the laboratory. The orbit of the Earth will cause this velocity to oscillate, making $f(\omega)$ sharper in December and broader in June,²² as can be seen along the time axis in Fig. 4. The function $f(\omega)$ can be thought of as the line shape of the axion signal, as measured by any experiments

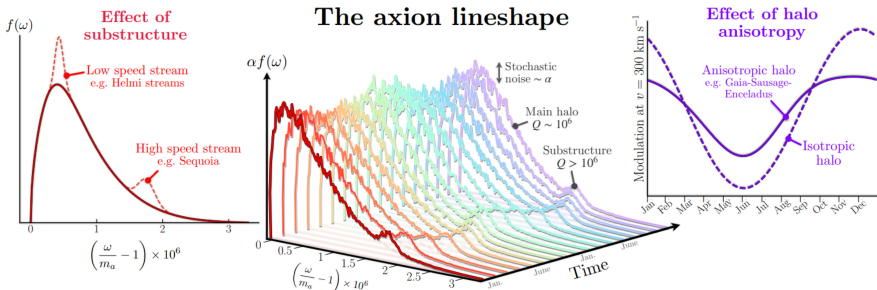


Fig. 4. The axion line shape $f(\omega)$ as a function of frequency ω relative to the axion mass, m_a . The typical width of the lineshape for a Maxwellian speed distribution is around $Q = m_a/\Delta\omega \simeq 10^6$, which sets the effective quality factor of the signal. The annual modulation of the Earth’s velocity acts to vary the width of the lineshape over the course of the year (the central plot covers a duration of two years). To the left and right of the central line shape plot, we show two potentially interesting modifications that are discussed in the text. Left: The effect of distinct accreted substructures that would contribute additional peaks to the lineshape. Right: The effect of anisotropy in the dark matter velocity distribution. An isotropic halo would generate a perfectly sinusoidal modulation signal, whereas any anisotropy would generate nonsinusoidal features. Courtesy of Ciaran O’Hare.

reliant on axion-photon conversion. It therefore serves as a signal model for the majority of both resonant and broadband haloscopes. Notable exceptions include experiments that are sensitive to length scales larger than the axion's coherence length,²³ and experiments that couple to the gradient of the axion field,^{23,24} for which velocity (i.e. directional) effects are important.

The simplest astrophysical ingredient to Eq. (2) is the dark matter density, which simply scales the amplitude of the signal power independent of frequency. We have a number of observational handles on the amount of dark matter in the solar neighborhood that rely on either the kinematics of nearby stars, or the construction of a global mass model for the galaxy (see Ref. 25 and references therein). Results from the two approaches are in broad but not exact agreement since they are still dominated by systematic uncertainties. With the recent map of 1.8 billion nearby stars collected by the Gaia mission,²⁶ the next few years will likely bring further improvements to our understanding of dark matter around us. For now, a recommended range of values is $\rho_{\text{DM}} \simeq 0.3 - 0.5 \text{ GeV cm}^{-3}$.²⁵

While it is expected under a purely cold dark matter scenario that there should not be significant fine-grained fluctuations in the local density on the milli-pc scales probed by experimental campaigns,²⁷ it remains to be robustly shown if this is also true for axionic dark matter. In particular, the astronomical-unit-scale clustering of axions seen generically in simulations of the post-inflationary scenario^{28,29} could radically alter the simple picture of a smooth dark matter distribution.^{30,31} Unlike dark matter density, we have no direct methods of measuring the velocity distribution. We can only make educated guesses about its general properties using simulations and the Milky Way's stellar halo as guides. The spherically symmetric and isothermal assumptions that form the basis of the SHM are reasonable starting points for devising a simple benchmark model, but are unlikely to be accurate in detail.³²

There are several ways in which the true dark matter distribution could be more complex. One of the most interesting of these in the context of axion experiments is the possibility of substructure. Elongated and kinematically cold streams of stars are observed abundantly around the Milky Way,³³ and our inner halo seems to be rife with accreted stars.^{34,35} It is natural to expect then that a fraction of our local population of dark matter might mirror these substructures. Two interesting features of the local halo that have been discovered and rediscovered using several independent data sets and substructure-finding techniques, are the so-called Sequoia^{36,37} and Helmi streams.³⁸ The Sequoia is a high-energy, retrograde feature, whereas the Helmi streams are largely prograde. If we were to make the assumption that the stellar material in these substructures can serve as a rough guess as to the kinematics of their dark matter components, then these two streams would show up as additional peaks in the axion line shape at high and low frequencies, respectively (shown in Fig. 3-1, left). The peak from the Helmi streams in particular would coincide with the maximum of the main axion line shape, so would potentially enhance experimental sensitivities. However, incorporating these substructures into a signal model would be premature without further dedicated simulations to understand their potential dark matter components.

Another post-Gaia revolution in our understanding of the Milky Way's formation is the discovery of a huge population of stars brought in during a significant merger around 8–10 billion years ago. This event, and the ancient dwarf galaxy it is associated with, were dubbed variously the Gaia-Enceladus³⁹ or Gaia-Sausage,⁴⁰ with amalgamated names like Gaia-Sausage-Enceladus (GSE) becoming increasingly popular. The debris of this collision is observed today as a population of halo stars in a triaxial figure⁴¹ out to around 20 kpc⁴² from the galactic center, and on highly radial (i.e. eccentric) orbits. This event likely brought in additional dark matter as well, meaning that part of the velocity distribution of axions around the Earth would also be strongly anisotropic in the galactic radial direction (i.e. a wider distribution along an axis perpendicular to the dark matter wind). Evidence from simulations,⁴³ as well as halo-shape arguments,³² both hint that around 20% of the Milky Way's dark matter was brought in by the GSE. At the level of the instantaneous axion line shape, the impact of the GSE would be very minor since directional information is integrated over. However, it would lead to measurable distortions to the annual modulation. The SHM has a perfectly sinusoidal time dependence, whereas any level of anisotropy would generate frequency-dependent nonsinusoidal features,³² as shown in Fig. 4 (right).

The conclusion for now seems to be that our understanding of the local dark matter halo is sufficient for running axion experiments with confidence. Certainly this is the case for the pre-inflationary axion, although understanding the late-time consequences of miniclusters formed in the post-inflationary scenario should be a priority. Line shapes that are sharper are easier to detect. So to remain conservative with regard to astrophysical uncertainties, experiments should not assume dark matter densities higher than, say, 0.5 GeV cm^{-3} , or speed distributions that are substantially colder than the SHM, which has a width of $\sigma_v = 167 \text{ km s}^{-1}$. The recent Gaia survey is revolutionizing our understanding of the Milky Way's halo, and there are many exciting features that are being unravelled. The possibility that one day an axion observatory could contribute to this ongoing astronomical revolution by measuring the dark counterpart of the Milky Way's halo is, therefore, rather exciting.

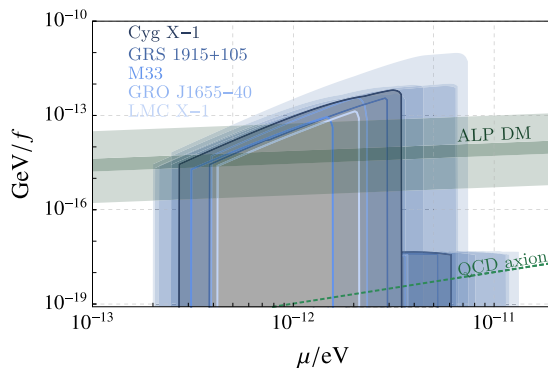
3.2. *Black holes and axions: From gravitational waves to axionic beacons (Masha Baryakhtar)*

If ultralight axions exist, fast-spinning black holes will superradiate: lose energy and angular momentum to exponentially growing bound-states of axions.⁴⁴ Rotating black holes thus source 'clouds' of weakly coupled bosons, independently of cosmological abundance. The fastest growth rates occur when the particle's Compton wavelength is comparable to the black hole radius; stellar mass black holes could probe axions in the range 10^{-14} – 10^{-10} eV.^{45–50}

The large energy density in the axion cloud can act as a source of gravitational and axion waves, which are approximately monochromatic with frequency set by (twice) the axion mass.^{45,46,51} For very weakly coupled particles, including the QCD axion, the

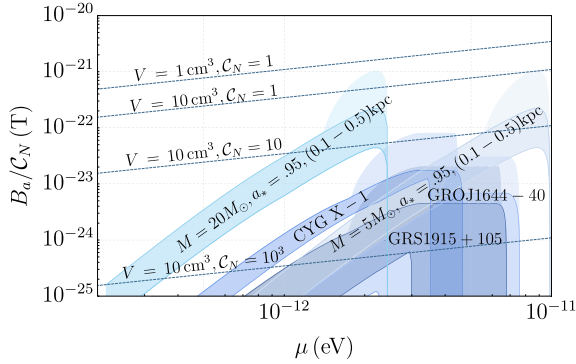
axion cloud depletes on long timescales through gravitational wave (GW) emission; signals can range from long (10^3 – 10^9 years), which are weak and only detectable from our galaxy, to short (days to months), and may be observable from black hole remnants of compact object mergers.⁴⁹ These signals fit into the general framework of continuous gravitational wave searches at LIGO/Virgo, and GW searches are ongoing.^{52–55} The expectation is that multiple galactic black holes would source detectable signals, clustered at frequency around twice the axion mass.^{49,54}

If axion self-interactions are important, new processes arise.^{45,56–59} Black hole energy sources the cloud through superradiance, which then evolves through self-interactions, a range of dynamics for different axion self-interactions with different observational implications. At fixed mass, from weakest to strongest interactions, there are four distinct behaviors.⁵⁸ (1) Gravitational superradiance: the cloud forms through black hole superradiance and is depleted through gravitational waves. The signatures are black hole spindown and gravitational waves at twice the axion mass. (2) Small self-interactions: black hole sources the initial cloud; further axion levels populate through self-interactions. The signatures are gravitational waves at twice the axion mass and lower frequency gravitational waves emitted from transitions between levels, and black hole spindown. (3) Moderate self-interactions: axion interactions dominate energy loss in the cloud (emission into black hole and to infinity), resulting in reduced occupation numbers. The signatures are weak gravitational waves, slower spindown and axion waves. (4) Large self-interactions: emission to infinity and into black hole leads to quasi-equilibrium of two levels; a smaller axion cloud parametrically slows the spindown of the black hole. There is no spindown on lifetimes of the age of the Universe, but there are long-lasting, monochromatic axion waves.



Source: From Ref. 58.

Fig. 5. Constraints on axion parameter space from black hole spin measurements in X-ray binaries. The “ALP DM” band corresponds to the range of quartic couplings that allow the observed dark matter abundance to be produced by the misalignment mechanism. The darker middle band corresponds to $\mathcal{O}(1)$ values of the initial misalignment angle ($\theta \in (1, \pi - 1)$), while the lighter bands above and below correspond to “tuned” initial values ($\theta \in (10^{-1}, \pi - 10^{-6})$).



Source: From Ref. 58.

Fig. 6. Axion waves signal amplitude in a nuclear-magnetic-resonance-type experiment from nearby black holes.

Existing measurements of black hole spins and masses are used to constrain axion parameter space (see Fig. 5). As self-interactions increase, spin extraction from the black hole slows, resulting in a weaker bound.

The axion wave signal is similar to axion dark matter; the nonrelativistic ($v/c \sim 0.01 - 0.1$), coherent axion waves are emitted at constant amplitude throughout the black hole lifetime. If axions couple to the Standard Model particles, the waves can be detected directly. Although the signals are weaker than those of axion dark matter, they can be enhanced for derivative axion couplings due to the larger velocity, they are more coherent and do not rely on axions being the dark matter.⁵⁸ Signal detection requires different data analysis strategies; open axion parameter space can give many potential signals, including from known rapidly rotating black holes (see Fig. 6).

4. Current Dark Matter Axion Searches

Experimental axion searches, especially based on the axion haloscope design, have enjoyed a renaissance over the last decade. The ADMX detector demonstrated the first sensitivity to DFSZ (Dine–Fischler–Srednicki–Zhitnitsky)-coupled dark matter axions, and a number of similar haloscopes have begun operating with sensitivity to the KSVZ (Kim–Shifman–Vainshtein–Zakharov)-coupled dark matter axions. More searches are being built or planned. New ideas about resonator design are opening up new mass ranges, both higher and lower, for exploration. Simultaneously, complimentary searches probing axion–nucleon and axion–electron couplings are also being developed. The status and prospects of these experiments dominated the preponderance of discussions during the workshop. Time constraints limited the presentations to only a representative sample of each technology among the currently operating searches.

4.1. Probing the axion–electron and axion–photon couplings with the QUAX haloscopes (Caterina Braggio)

We describe recent results obtained within the QUAX (QUaerere AXions) collaboration, for the development of haloscopes based on the axion–electron (QUAX ae) and axion–photon (QUAX $a\gamma$) interactions. Planned activities for 2021–2025 years at the LNL and LNF National INFN laboratories (Italy) are also mentioned.

Introduction

The most sensitive instruments to explore the parameter space of the QCD axion are the haloscopes, which rely on axion-to-photon conversion within microwave cavities under multi-Tesla fields.⁶⁰ Since the axion mass is unknown, all possible mass ranges need to be explored, and experimental efforts are made to enhance the speed at which haloscopes can scan through parameter space at some fixed axion-to-photon coupling g_γ . Interaction of the axion with the electron spin has also been analyzed in QCD axion models, but it is harder to exploit for detection as it is weaker than the axion–photon coupling. Based on the work by Barbieri *et al.*⁶¹ in 2017, we proposed a ferrimagnetic haloscope that can probe the axion-electron parameter space with the required sensitivity, provided some experimental requirements are satisfied.⁶² This is a challenging experiment as it concerns both the magnetic material properties and signal readout. Here, we report the most relevant results obtained with the demonstrator we built. In addition, we describe the current experimental efforts to realize haloscopes based on the axion–photon conventional approach in the 8.5–11 GHz frequency range.

The QUAX ae haloscope

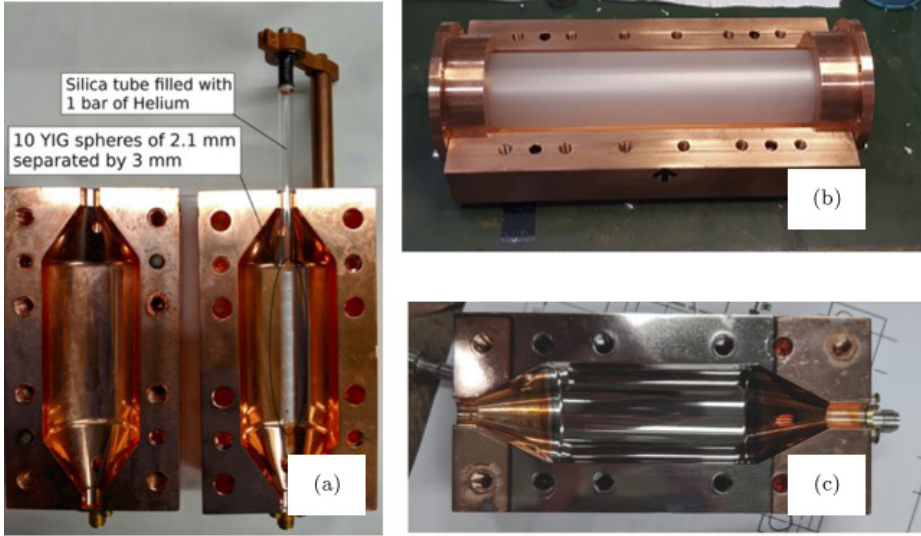
The axion–electron interaction can be expressed in terms of an effective magnetic field interacting with the electron,⁶¹ with amplitude B_a and frequency ν_a :

$$B_a \simeq 5 \times 10^{-23} \frac{m_a}{50 \mu\text{eV}} \text{ T}, \quad \nu_a \simeq 12 \frac{m_a}{50 \mu\text{eV}} \text{ GHz},$$

where m_a is the axion mass in eV.

To detect the field B_a , a magnetic material with highest spin density n_s and narrow linewidth (i.e. long spin–spin relaxation time) is devised, such as yttrium iron garnet (YIG). The uniform magnetization mode is coupled to a microwave cavity mode to realize the optimal transducer.^{63,64} The power deposited in the hybrid resonator is collected with an antenna and readout with a conventional heterodyne receiver, possibly with a Josephson Parametric amplifier as the first stage of amplification to minimize electronic noise.

While secondary issues have been addressed, including ppm level uniformity and high stability of the 2T magnetic field, current experimental challenges are: (1) the required sample volume of about 100 cm³ has to be hosted in high frequency cavities (40–50 GHz); and (2) the ferrimagnetic resonance linewidth should be as low as 150 kHz, corresponding to a relaxation time of 2 μ s. The best value we obtained up to



Source: Adapted from Ref. 73.

Fig. 7. (a) Cavity hosting the magnetic material used in the QUAXae experiment. Courtesy of Caterina Braggio. (b) Dielectric resonator (from Ref. 67) and (c) superconducting (NbTi film) hybrid cavity used for the QUAXae haloscopes (from Ref. 73).

now is of $0.3 \mu\text{s}$, improving on previous realizations thanks to a procedure we developed to get high quality YIG spheres.⁶⁵ This scheme, which has excellent prospects for model discrimination in the event of discovery, has been used for a preliminary axion dark matter search based on a photon–magnon hybrid system consisting of 10 small spheres of YIG (Fig. 7(a)) coupled to a cylindrical cavity mode.⁶⁶ To improve on the reported limit of the axion–electron coupling constant, not only significant R&D activities are required on magnetic materials and hybrid magnon–photon systems, but capability of single-magnon readout based on superconducting transmon qubits is also necessary.

QUAX $a\gamma$ haloscopes

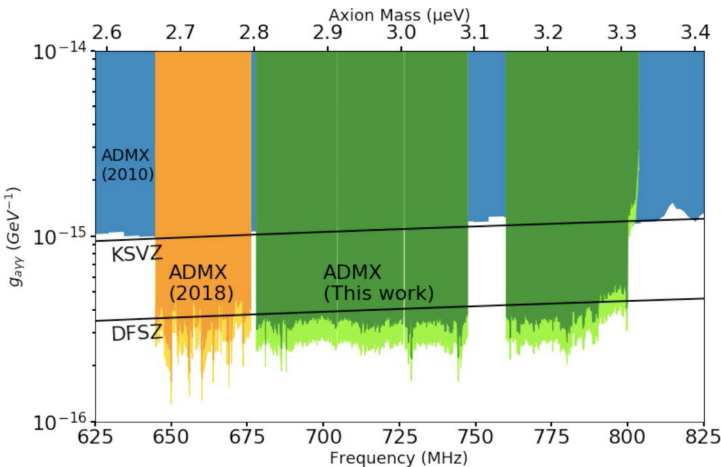
As for the axion–photon haloscope, we address the challenging high-frequency range 8.5–11 GHz. The LNL and LNF-INFN laboratories will work in synergy, operating in complementary mass ranges on different cavity resonator technologies. At LNL, a dielectric resonator will be used⁶⁷ for 9.5–11 GHz, whereas in LNF a multicavity experiment is devised to probe the 8.5–10 GHz range. The QUAX $a\gamma$ collaboration has recently published the results of the last-run data analysis, with sensitivity to axion–photon coupling only a factor 5 from KSVZ benchmark models⁷³ at $37 \mu\text{eV}$ mass (9.08 GHz frequency). A copper resonator coated with a Nb–Ti film produced by magnetron sputtering has been used for this search (see Fig. 7(b)), whose quality factor under the applied magnetic field of 2 T was five times higher than in copper.⁶⁹

4.2. Wavelike dark matter on the horizon: Searching for the DFSZ axion with the ADMX haloscope (Chelsea Bartram)

The QCD axion is an appealing dark matter candidate for its unique ability to simultaneously account for the missing mass and solve the strong-CP problem. Pierre Sikivie first proposed a method for detecting the QCD axion called the resonant haloscope, and searches have been ongoing since. Notable among these is the ADMX detector. Recent developments in quantum science and cryogenics have enabled ADMX to greatly lower noise and become the only resonant haloscope sensitive to the DFSZ axion over a wide axion-mass range.

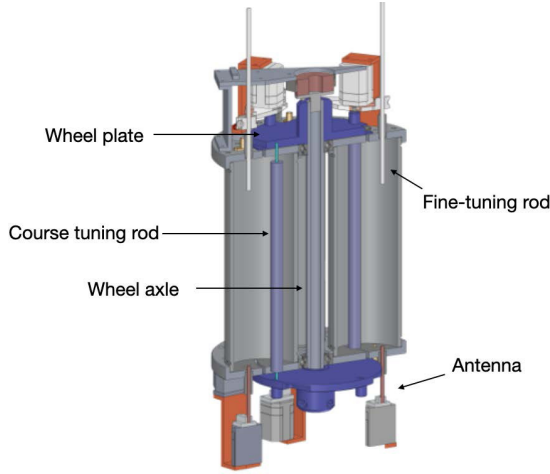
Details from the prior ADMX run (680–790 MHz) were presented, including results from an in-depth analysis and instrumentation paper (see Fig. 8). Preliminary results from ADMX included scanning progress through the 800–1020 MHz frequency range, demonstration of a traveling wave parametric amplifier (TWPA) for higher frequency wide-band operation, and testing of a resonant feedback setup on a prototype cavity located within the ADMX insert.

In the near term, ADMX plans to implement a low-volume cavity with a larger tuning rod. Following this, scanning of higher frequencies will require a series of multicavity array searches. The first will use a four-cavity array located at the University of Washington (see Fig. 9). The next will be sited at Fermilab and enable frequencies up to 4 GHz to be searched. Research and design work for forthcoming axion search concepts are propelled by ADMX collaborators at various institutions. A variety of options are under consideration for future ADMX searches, including single-photon counting with qubits (Fermilab), broadband microwave antenna



Source: From Ref. 70.

Fig. 8. “Limit plot” showing DFSZ exclusion limit at 100% dark matter density for prior two data-taking runs.



Source: From Ref. 78.

Fig. 9. Rendering of the 1.4–2 GHz multicavity array to be sited at the University of Washington.

designs (Fermilab), and the implementation of programmable filters on field-programmable gate array boards in resonant feedback systems (University of Sheffield). To the extent that it is possible, some concepts for future searches were deployed and tested within the current insert, such as the TWPA, piezo motors and prototype of the resonant feedback system on the ADMX sidecar cavity.

4.3. Lumped-element searches for low-mass axion dark matter (Chiara P. Salemi)

Axions were hypothesized several decades ago as a part of the solution to the strong CP problem and have long been known to be an excellent dark matter candidate.^{4,5,71,72,79–81} Despite their long-standing strong theoretical motivation, laboratory experiments have probed only small portions of their possible mass range. Recent theory work has further motivated searches over a wide range of masses, $10^{-12} \lesssim m_a \lesssim 10^{-1}$ eV.^{73–75}

At the lower end of this mass range ($m_a \lesssim 1 \mu\text{eV}$), the axion wavelength is long relative to a reasonable detector size, motivating a lumped-element detection scheme to search for axion–photon interactions.⁷⁶ This method is based on an LC circuit where the individual components can be treated as lumped-circuit elements under the magneto-quasistatic approximation. In this circuit picture (see Fig. 10), the axion signal can intuitively be thought of as an effective current,

$$\mathbf{J}_{\text{eff}} = g_{a\gamma\gamma} \sqrt{2\rho_{DM}} \cos(m_a t) \mathbf{B} \quad (3)$$

that can inductively couple into a pickup structure. Note that the effective current oscillates with frequency m_a and is proportional to \mathbf{B} , the magnetic field that sources the axion interaction. An oscillating real current induced on the pickup can then be

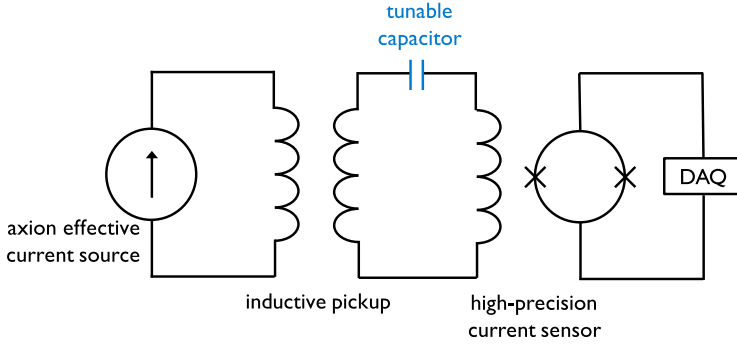


Fig. 10. Circuit diagram for a lumped-element axion detector. In the presence of an external magnetic field, the axion field acts as an effective current source. A pickup structure can inductively couple to this effective current, generating a real current that can be detected with high-precision sensors such as SQUIDs. By including a tunable capacitor in the detection circuit, the signal strength can be magnified by the Q-value of the resulting tunable LC resonator. Courtesy of Chiara P. Salemi.

detected using high-precision sensors such as superconducting quantum interference devices (SQUIDs). The pickup can be entirely inductive for a broadband readout or, with the addition of a tunable capacitor, can operate as an LC resonator that can scan over the possible axion masses. Operating in resonant mode provides an enhancement of the signal strength by the resonator quality factor, ultimately improving the overall experimental sensitivity for a given run-time.⁷⁷

Three first-generation lumped-element axion experiments have demonstrated the viability of this technique and have set world-leading limits on low-mass axions, shown in Fig. 11. Two of these, ABRACADABRA-10 cm and SHAFT, used a

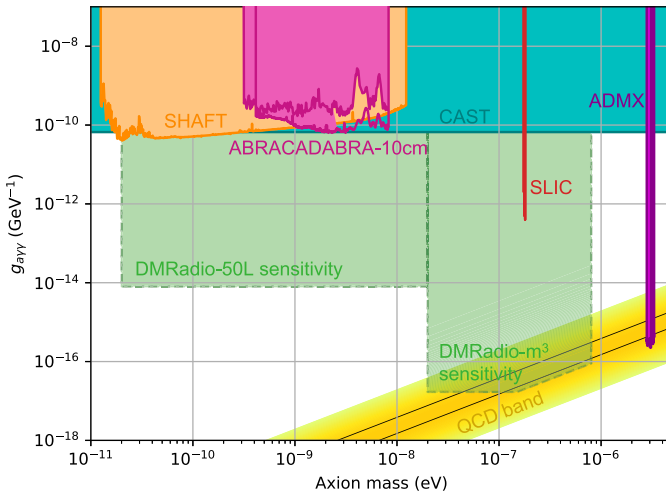


Fig. 11. Recent limits on the axion–photon coupling using the lumped-element detection method. Also shown are the sensitivity projections from two upcoming experiments, DMRadio-50L and DMRadio-m³, the latter of which will probe the QCD axion band at DFSZ sensitivity. Courtesy of Chiara P. Salemi.

toroidal magnet to source the effective axion current. The toroidal geometry provides a field-free region in the central hole for the inductive pickup structure and readout electronics. Both experiments opted to use a broadband readout for their first-generation setup. SHAFT and ABRACADABRA-10 cm have together excluded axion-like particles over a wide range of masses, $10^{-11} \lesssim m_a \lesssim 10^{-8}$ eV, with axion-photon couplings $g_{a\gamma\gamma} \gtrsim 10^{-11}$ GeV $^{-1}$.^{82–84}

The third first-generation experiment, ADMX-SLIC, used a solenoid magnet, which suffers from a high field in the region of interest, but is easier to build. SLIC also used a superconducting resonant readout, allowing it to reach a high sensitivity, $g_{a\gamma\gamma} \gtrsim 10^{-13}$, over a narrow range of masses, $m_a \approx 10^{-7}$ eV.⁵

These experiments have paved the way for future, large-scale, lumped-element axion searches. The next-generation experiment is DMRadio-50L, which is about to start construction. It will use a resonant readout with a ~ 50 L toroidal magnet and will search for axion-like particles over a much larger parameter space, shown in Fig. 11. Another larger experiment, DMRadio-m³, is currently being designed and is expected to probe DFSZ axions at slightly higher masses, $m_a \approx 10^{-7} - 10^{-6}$. DMRadio-m³ will also be a resonant experiment and will likely be a solenoid design to avoid parasitic resonances that appear at higher frequencies with the toroid. In addition, R&D efforts are underway with the goal of eventually building an experiment that would reach DFSZ sensitivities down to $m_a < 1$ neV.

A recent set of first-generation experiments have demonstrated that the lumped-element method is a viable and promising technique for axion detection. Building on these successes, new experiments are underway to probe the interesting and so far unexplored parameter space of light axion-like particles and QCD axions. Lumped-element detection at low masses is a vital component of the larger program to search for axion dark matter over its entire mass range.

4.4. Axion search activities at IBS/CAPP (Soohyung Lee)

The Center for Axion and Precision Physics Research of the Institute for Basic Science (IBS/CAPP) runs several axion search experiments. It has four systems for the experiments: two dry-type dilution refrigerators equipped with 8 T superconducting magnets of 125 mm (referred to as “8 T/125 mm”) and 165 mm (referred to as “8 T/165 mm”) clear bores, a wet-type dilution refrigerator equipped with a 12 T superconducting magnet of 320 mm clear bore (referred to as “12 T/320 mm”), and a wet-type refrigerator with a 9 T superconducting magnet of 125 mm clear bore (referred to as “9 T/125 mm”).

With three systems among them, prototype experiments with high-electron mobility transistor amplifiers were done: the 8 T/165 mm scanned an axion frequency range of 1.60–1.65 GHz at $4 \times g_{a\gamma\gamma}^{\text{KSVZ86}}$ where $g_{a\gamma\gamma}^{\text{KSVZ}}$ is the axion-photon coupling for the KSVZ axion¹³⁴, the 8T/125mm searched 2.457–2.749 GHz at $9 \times g_{a\gamma\gamma}^{\text{KSVZ}}$ and 2.5903–2.5918 GHz at $g_{a\gamma\gamma}^{\text{KSVZ87}}$; and the 9T/125mm explored 3.14–3.36 GHz at $10 \times g_{a\gamma\gamma}^{\text{KSVZ135}}$ with realizing the first multiple-cell microwave resonant cavity.⁹³

The 12 T/320 mm system is dedicated for the flagship experiment to search for axion frequency range of 1–4 GHz at the sensitivity for the DFSZ axion, $^{88}g_{a\gamma\gamma}^{\text{DFSZ}}$. The experiment employs a microwave resonant cavity of 30 L and Josephson-junction parametric amplifier (JPA).⁸⁹ In the first year of the experiment, it will scan 1.0–1.4 GHz at below $g_{a\gamma\gamma}^{\text{KSVZ}}$ sensitivity, and it will reach $g_{a\gamma\gamma}^{\text{DFSZ}}$ for 1.0–2.0 GHz. It will also expand to 2–4 GHz at $g_{a\gamma\gamma}^{\text{DFSZ}}$ later on.

A breakthrough to maximize the cavity volume for the prototype systems scan rate⁹⁰ is the phase matching,⁹¹ which integrates the systems with more benefit than a statistical integration. For this integration, the 9 T/125 mm system will be replaced with a dry-type dilution refrigerator with a 12 T superconducting magnet of 96 mm clear bore. Combining those, the total effective volume of the experiment is expected to be 6.2 L. Individual experiments are being built for 5.5–6.0 GHz targeting $g_{a\gamma\gamma}^{\text{KSVZ}}$ with six- and eight-cell cavities for 8 T/125 mm and 8 T/165 mm, respectively. The phase-matching experiment will eventually cover 4–6 GHz at $g_{a\gamma\gamma}^{\text{KSVZ}}$. Even further, a realization of a superconducting cavity⁹² will be another breakthrough to achieve $g_{a\gamma\gamma}^{\text{DFSZ}}$.

The IBS/CAPP is now one of the players in the axion search race. It pursues to search 1–8 GHz at $g_{a\gamma\gamma}^{\text{DFSZ}}$ with microwave resonant cavities and other breakthroughs such as JPA, phase-matching and superconducting cavity. The frequency range will be extended to even higher frequencies with realizing a single-photon detector in the future.

4.5. Axion program at the University of Western Australia (Michael E. Tobar)

4.5.1. ORGAN

In recent years, interest has grown in searching the high mass ($> \sim 50 \mu\text{eV}$) range for dark matter axions.⁹⁴ The interest is due to a range of promising theoretical proposals^{96,149} suggesting axions could exist in this range. Despite this, there are few experiments that propose to scan this range, owing in part to a host of technical difficulties associated with conducting axion detection experiments at higher frequencies. The ORGAN Experiment is a high-mass, (Sikivie-style) axion haloscope hosted at the University of Western Australia. Since 2016 we have conducted R&D, prototyping, path-finding, planning and commissioning for the ORGAN Experiment, which will probe this range.¹³⁶ This work culminated in the first experiment in this mass region in 2017. Subsequently, we have undertaken future planning for the experiment, and have already commenced long-term operation in 2021.

The experiment will run for 7 years, from 2021 to 2027, with the axion mass range of interest of $\sim 60\text{--}200 \mu\text{eV}$, corresponding to roughly 15–50 GHz in photon frequency. To overcome the significant technical challenges associated with operating a traditional resonant cavity haloscope, we pursue four avenues of research and development. First, we consider novel resonator designs based on higher-order modes in resonant cavities and dielectric materials, to increase form factors and volumes at

high frequency.^{136,137} Second, we investigate novel schemes for combining multiple resonators, such as cross-correlation,⁹⁷ to increase effective detector volume. Third, we consider high critical field superconducting coatings to increase quality factors of resonators.^{98,99} Finally, we propose to implement promising single-photon counting technologies and/or subquantum limited linear amplification.¹⁰⁰ The experiment will consist of two phases, each broken into stages. Phase 1 will consist of two targeted scans at 15–16 and 26.1–27.1 GHz, whereas Phase 2 will consist of the entire 15–50 GHz region, broken into 5 GHz stages.

All phases of the run plan will operate at mK temperatures, in a 14 T (or higher) magnetic field, at the University of Western Australia. The scans will use a signal-to-noise ratio of 4 as the target for searching, and will achieve different levels of sensitivity depending on success of various aspects of R&D during the 7 years of the experiment.

4.5.2. UPLOAD

The UPLOAD-MC (UPconversion Loop Oscillator Axion Detection with a Microwave Cavity) experiment is similar to traditional haloscopes. It is the first in a new class based on frequency metrology,^{101,102} instead of power detection. Most haloscopes attempt to create photons by interacting axions with a virtual photon source, but the Primakoff process also generates products in the presence of real photons, as first noted by Sikivie in 2010.¹⁰³ AC haloscopes based on the two-photon process are capable of detecting axions near the sum and different frequencies of two photonic oscillators. The method implemented here allows detection via precision frequency measurements causing modulations as opposed to photon generation.^{103–105} Moreover, precision oscillators of the type proposed here have been used in the past for some of the best tests of fundamental physics, including variations in fundamental constants and local position invariance,^{106,107} as well as tests of Lorentz invariance violation,¹¹³ with proven long-term performance of up to eight years,¹⁰⁹ and if designed properly the sensitivity will be determined by the white noise frequency floor of the frequency stabilization system.¹¹⁰ In particular the University of Western Australia team members leading this project are world experts in developing low-noise microwave and radio-frequency oscillators^{111,115} based on low-noise phase detection,¹¹² and using them to test fundamental physics.^{108–110,113,114,116,117} This is evidenced by the fact that the technology developed in their lab is now present in all of Raytheon’s defence radar.¹¹⁸

4.5.3. BEAST

When axions, $a(t)$, mix with an applied photonic degree of freedom (γ), a photon of different frequency will be produced via a second photonic degree of freedom (γ') through the inverse Primakoff effect, given by $\gamma + a \rightarrow \gamma'$. From the view point of the second photon degree of freedom, γ' , this is a nonconservative electro-dynamical process due to the creation of photons from an external nonelectromagnetic source (namely the first photonic degree of freedom mixing with the axion). If the first

photonic degree of freedom is an applied DC \vec{B} -field, the modified axion electrodynamical equations become similar to the electrodynamics of an AC voltage source, producing an AC electromagnetic action (or emf, $\mathcal{E}_a(t)$) oscillating at the Compton frequency of the axion. As in standard electrodynamics, $\mathcal{E}_a(t)$ may be modeled as an oscillating effective-impressed magnetic-current boundary source. This boundary source is present in the axion–photon electrodynamical equations^{119,120}; however, the relevant term is usually approximated to equal zero, so only a derivative axion–photon coupling remains, consistent with a zero total derivative. In the low-mass limit where the Compton wavelength of the axion is greater than the dimensions of the experiment (quasi-static limit), this approximation is no longer valid and the boundary source terms are the dominant effect. The end result is the realization of new Broadband Electrical Action Sensing Techniques (BEAST), with a sensitivity linearly proportional to the axion–photon coupling.^{119–121}

Contrary to what has been published by others,^{122–124} we have subsequently shown our sensitivity calculations are consistent, and calculate that the electric field produced by the axion current in the low-mass limit is suppressed. *Our technique does not detect this suppressed axion-induced electric field, $E_a(t)$, but directly detects $\mathcal{E}_a(t)$ from the nonconservative process.* This is a much more sensitive technique because it is not suppressed by the mass of the axion and puts axion–photon coupling low-mass experiments on a similar footing to axion–gluon coupling experiments,^{125,138} such as the CASPEr^{100,132} and Sussex-RAL-ILL nEDM experiments,¹²⁷ which are not suppressed by the axion mass and have also been projected to be sensitive enough to detect QCD axions at low mass ranges below 10^{-8} eV. This result may be considered controversial, but no one has yet shown how this calculation is wrong. To fully consider this effect in axion electrodynamics, the electrodynamics of standard impressed sources that convert external energy to electromagnetic must be fully understood.^{128–131} Adding the impressed source is similar to standard electrodynamics where the vector curl of a polarization vector is nonzero, this is also consistent with applying the Minkowski Poynting vector to the problem,^{132,133} otherwise applying the Abraham Poynting vector applied to this case will miss the effect of $\mathcal{E}_a(t)$ as an impressed source.

This work was funded by the ARC Centre of Excellence for Engineered Quantum Systems, CE170100009, and Dark Matter Particle Physics, CE200100008.

4.6. *Post-inflationary axion dark matter search with a dielectric haloscope (Chang Lee)*

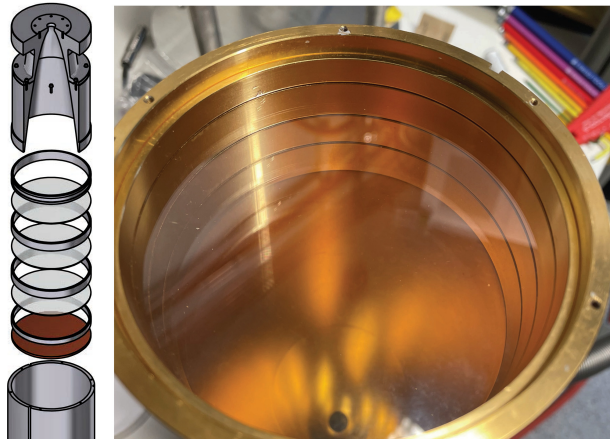
The QCD axion is an ideal candidate for CDM¹³⁹ and a solution to the strong CP problem.⁷¹ Recent lattice QCD calculations predict a mass heavier than $26 \mu\text{eV}$ if axions are generated after cosmic inflation.¹⁴⁰ Unfortunately, this range is slightly beyond the reach of current-generation axion search experiments that use axion’s coupling to a resonant cavity’s fundamental mode.^{141,150}

The MADMAX collaboration proposes to probe post-inflationary QCD axion using a dielectric haloscope.^{142–144} A dielectric haloscope measures traveling waves

induced by the axion field at boundaries of different media. The signal power increases when the impedance of a receiver matches that of a mirror surface via dielectric layers. A low-reflecting taper or antenna collects the signal. The taper or antenna reflects very little and supports fewer unwanted standing wave modes. The traveling wave detection structure, what we call the “leaky resonator,” distinguishes a dielectric haloscope from cavity detectors^{136,145,151} that detect standing-wave modes between reflecting boundaries.

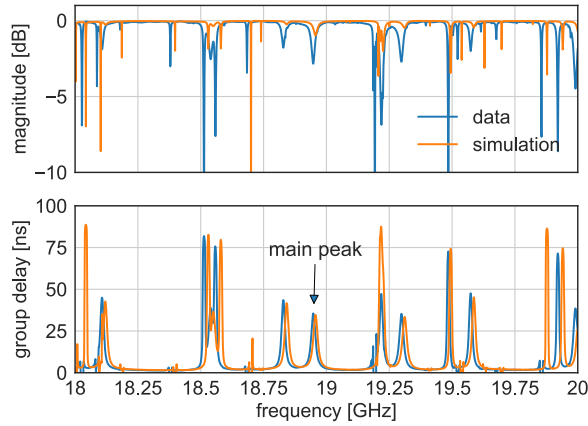
A small proof-of-principle dielectric haloscope is in development. It consists of a copper mirror and three sapphire disks (100 mm in diameter), as shown in Fig. 12. The dielectrics boost the axion-induced traveling wave power at 19 GHz, more than 2000 times that of the single metallic mirror alone. The metallic spacing rings and the gold coating on the disks’ rims define lateral boundaries. A parabolic taper¹⁴⁶ transforms the TE_{11} mode of the booster to that of the waveguide. Figure 13 shows that room-temperature reflectivity measurement agrees with simulation. A similar measurement at liquid helium temperature is ongoing. Assuming 11 K system temperature, 90% efficiency, and a signal-to-noise ratio of 5, a 7-day measurement can probe hidden photon kinetic mixing χ below 10^{-13} within a bandwidth of 20 MHz around 19 GHz, corresponding to a hidden photon mass of $78.85 \mu\text{eV}$.

The MADMAX (Magnetized Disc and Mirror Axion Experiment) collaboration is preparing a series of larger dielectric haloscopes. The prototype is an R&D platform that aims to test the system at a cryogenic temperature and in the 1.6 T magnetic field of the MORPURGO magnet¹⁴⁷ at CERN. The full MADMAX is planning to use a 9 T, 1.3-m bore magnet and probe the QCD axion at 40–400 μeV .



Source: From Ref. 148.

Fig. 12. (Color online) Left: The proof-of-principle dielectric haloscope consists of a copper mirror (brown disk) and three sapphire disks (transparent disks). Interchangeable aluminum rings set the distances between the disks. A parabolic taper (top) collects traveling waves exiting the resonator. Right: The assembled setup is seen from the mirror side. The mirror is not included in the assembly.

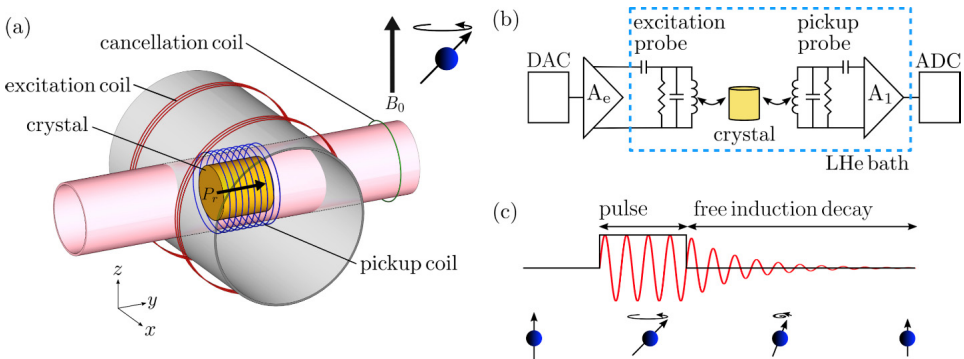


Source: From Ref. 148.

Fig. 13. Dielectric haloscope’s room-temperature reflectivity is compared against simulation. The top and bottom plots show reflectivity magnitude and group delay against frequency. The main resonance appears at 18.95 GHz. Surface current through the disks’ rims yields loss higher than simulated. Mode-crossing inside the taper yields other peaks.

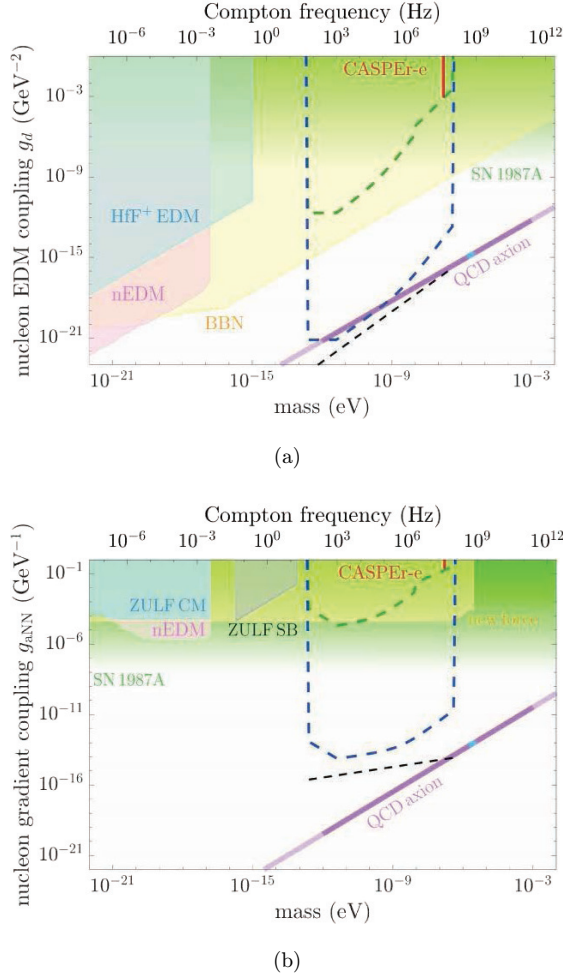
4.7. What is up, CASPER? (Dmitry Budker for the CASPER collaboration)

The Cosmic Axion Spin-Precession Experiment (CASPER) program that originated with the proposal⁹⁵ aims at the detection of galactic axions or ALPs via their couplings to nuclear spin. One such “gluon” coupling induces an electric dipole moment of nucleons, and the other results in nuclear spin precession in the gradient of the axion (ALP) field. Both effects are described by a time-dependent interaction oscillating near the Compton frequency of the particle and are searched for via nuclear magnetic resonance techniques. CASPER is presently a multi-institution



Source: Adapted from Ref. 95.

Fig. 14. Principles of CASPER-Boston.



Source: Adapted from Ref. 95.

Fig. 15. Summary of the results and future projections of the CASPER program.

international collaboration, with experimental activities concentrated at Boston University (USA) and Helmholtz Institute, Johannes Gutenberg University, Mainz (Germany).

In recent years, it has produced several constraints on the ALP parameter space in both couplings, in the mass range from 10^{22} to 1.7×10^7 eV, with the most recent one described. Figure 14 illustrates the principles of this experiment, while the results and projections of CASPER are shown in Fig. 15. It should be pointed out that there are a number of spinoff experiments, either complementing CASPER or looking for other couplings or other kinds of ultralight bosonic dark matter. Among these are the SHAFT experiment,⁸³ searches for oscillating fundamental constants in atomic

spectroscopy,¹⁵² hybrid networks cross-correlating the data from different types of dark matter sensors, dark matter searches with masers¹⁵³ and spin amplifiers,¹⁷⁴ as well as indirect searches via detection of exotic (“fifth-force”) interaction induced by virtual particles whose real counterparts could constitute some of the dark matter.

5. Non-Dark-Matter Axion Searches

It is possible that the axion exists, yet only makes up a small fraction of the cosmological dark matter. In this case, direct observation becomes much more challenging because the local density of dark matter cannot be relied upon as a copious axion source. Regardless, techniques do exist that may be able to detect the axion in this case. Detecting signatures of axions produced in the Sun, prospects for the so-called light-shining-through-wall technique and detecting axion-mediated forces between spin polarized objects were discussed at this workshop.

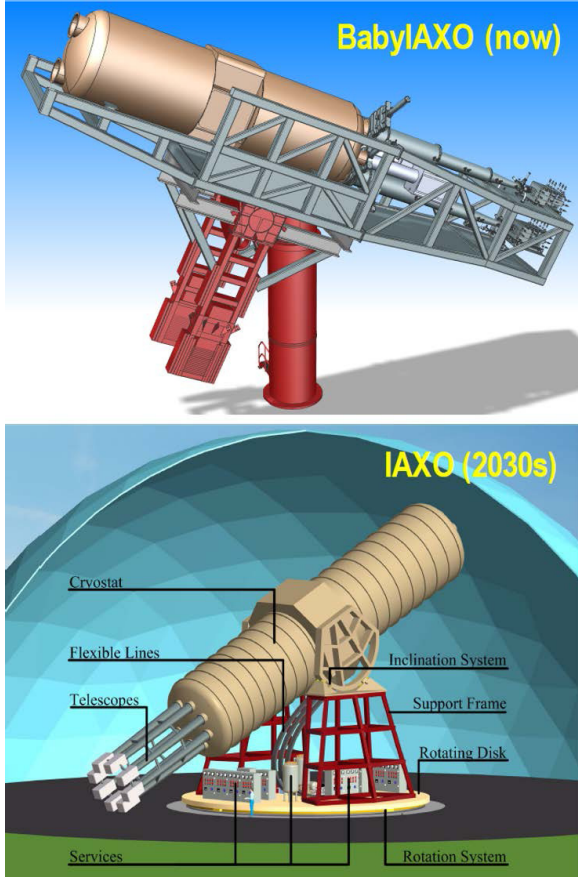
5.1. *The status of solar axion searches and the international axion observatory (IAXO) (Julia Vogel)*

Axions are neutral pseudo-scalar particles originally predicted to exist as a consequence to the PQ solution for the strong CP problem.^{71,80} They may be detected by their interactions to two photons through a loop of virtual particles. This interaction, known as the “inverse Primakoff effect”, can allow for axions to be converted into detectable photons. Axions can be either primordial in nature (direct dark matter searches) or generated initially from intense photon sources such as lasers or stellar objects like the Sun. Axion of the latter type can be studied using the helioscope technology, which was developed by Pierre Sikivie,⁶⁰ and relies on axions to be produced in the intense photon fields of the Sun where they carry the kinetic energy of the Sun’s thermal environment, which boosts their energies to keV scales. These axions would then stream out of the Sun and can be collected in a large dipole field on Earth where they can reconvert to detectable X-ray photons.

The first-generation helioscope was the Rochester–Brookhaven experiment that used a few hours of data using a 2.2 Tesla 1.8 m long magnet that took about 15 min of data a day while pointed at the Sun.¹⁵⁴ It was followed by the SUMICO second-generation experiment with a 4 Tesla, 2.3 m long magnet on a platform that could follow the Sun for about 12 h a day¹⁵⁵ and took data under vacuum as well as with helium gas in the magnetic field region. The helium gas enables the restoration of the coherence condition under which axions and photons are in phase and can reconvert into X-ray photon at higher axion masses, thereby extending the mass reach of the solar axion search. A third generation experiment, the CERN Axion Solar Telescope (CAST^{157,158}), was built using a decommissioned Large Hadron Collider prototype magnet (10 Tesla magnetic field over a 9.2 m length) and was able to follow the Sun for 3 h a day. This experiment operated with several advanced low-noise detectors, including a low-background Micromegas detector, along with a

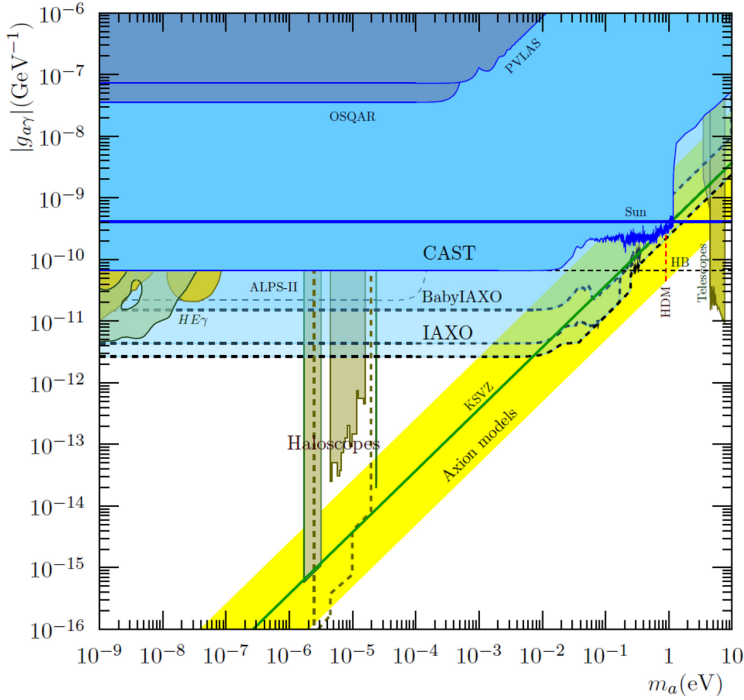
complementary set of X-ray-focusing optics coupled to a charged-coupled device camera, both flight spare instruments from different ESA space missions. It set broadband world-leading limits ruling out axions with mass below $m_a < 0.2 \text{ eV}$ and coupling above $g_{a\gamma} < 0.66 \times 10^{-10} \text{ GeV}^{-1}$.¹⁵⁶

The International Axion Observatory (IAXO^{159,160,184}) is a fourth-generation experiment that will have 1–1.5 order of magnitude higher sensitivity to axion couplings than CAST. Its current design calls for a toroidal magnet design, similar to that of ATLAS, with peak field of 2.5 T. It will allow for eight bores that are 20 m long. The lower magnetic field relative to CAST is more than compensated by 2.3 m² aperture from its 8 bores of 60 cm diameter each, which corresponds to a factor of 793 larger area than that of CAST. The system will be placed on a moving platform to allow operations 12 h a day following the Sun. A full design study of IAXO can be found in Ref. 184. An intermediate experiment, dubbed



Source: From Refs. 184 and 161.

Fig. 16. Sketches of the IAXO and BABY IAXO precursor experiment.



Source: From Ref. 161.

Fig. 17. IAXO and BABY IAXO expected sensitivities.

BabyIAXO,¹⁶¹ is in the near-term planning phase (the experiment is entering its construction phase in 2022) and is expected to consist of two 70 cm diameter bores of a 10 m long magnet and will allow testing of a variety of detector systems ahead of the full IAXO system (see Fig. 16) while at the same time significantly extending the physics reach over CAST (Fig. 17).

5.2. ALPS II (Aaron Spector)

The Any Light Particle Search II (ALPS II) is a light-shining-through-a-wall experiment taking place at DESY in Hamburg, Germany, that will search for axion-like particles with masses below 0.1 meV down to a coupling strength between axions and two photons of $2 \times 10^{-11} \text{ GeV}^{-1}$. These experiments use a high-power light source propagating through a dipole magnetic field to generate a beam of ALPs that travel through a wall and blocks the light. On the other side of the wall another strong magnetic field will reconvert a few of the ALPs back to photons.

To reach the targeted sensitivity, ALPS II will utilize two strings of 12 superconducting dipole magnets to generate an integrated magnetic field length of $560 \text{ T} \cdot \text{m}$ before and after the wall, along with high-finesse 122 m optical cavities that will increase the reconverted photon rate by up to 9 orders of magnitude. An

amplified nonplanar ring oscillator (NPRO) is used to seed the cavity before the wall with up to 50 W of laser light at a wavelength of 1064 nm. With these parameters, an axion-like particle with a coupling of $2 \times 10^{-11} \text{ GeV}^{-1}$ would then generate a photon rate of roughly a single photon per day. This will be measured by two independent single-photon detection schemes, a heterodyne detection system,¹⁶³ and a transition edge sensor counting single photons.¹⁶²

The operation of the high-finesse cavities requires that the laser light is free to propagate between the cavity mirrors while incurring optical losses below around 50 ppm. Since the magnets were formerly used to steer protons around the arcs of the HERA particle accelerator, they have a curvature that limits their free aperture to 37 mm. Therefore, all of the magnets underwent a straightening procedure that produced free apertures between 46 and 51 mm, sufficient to limit the losses from clipping on the magnet string to less than 1 ppm. The expected scattering losses from the mirrors that will be used in the initial science run were expected to be between 20 and 30 ppm per mirror, however initial results suggest they are roughly twice that amount. An optics upgrade is also planned after the first science run that will implement mirrors aiming at an even higher surface quality to further reduce the losses and increase the regenerated photon rate.

A sophisticated optical system must be used to maintain the coherence and the spatial overlap between the cavities before and after the wall in order to successfully boost the reconverted photon rate.¹⁶⁴ A series of phase-lock loops will be implemented that allow us to monitor any differential length changes between the cavities and ensure that the axion field is resonant in the cavity after the wall. This system relies on a central optical bench (COB), on which we interfere the transmitted fields from the cavities with a reference laser. This must be done while also preventing any stray light with power levels on the order of 1 photon per day from coupling between the cavities. The COB will also play a critical role in maintaining the alignment of the cavity optics. The mirrors at the center of the experiment are mounted directly to it, limiting the relative alignment drift between them. The COB also houses position sensors capable of monitoring the alignment noise of the mirrors at the end stations of the experiment.

Figure 19 shows a photo of the magnet string. All 24 magnets have now been installed, cooled-down and operated at full current, while the clean rooms that house the lasers and optics of the experiment are fully operational. While this work was being done, preliminary work was performed on the optical system using the full magnet-beam tube. This involved shining a HeNe laser through the 240 m magnet string to serve as an alignment reference for the optical system as is shown in Fig. 18.

Since then the COB has been fully assembled and installed in its vacuum chamber in the central station of the experiment. The cavity after the wall has also been fully commissioned and can be operated with a laser held on its resonance for indefinite periods of time. In addition to this, the full control system that stabilizes the frequency of the 50 W laser with respect to this cavity has been demonstrated and in November of 2022 light from this laser was measured in transmission of the cavity for

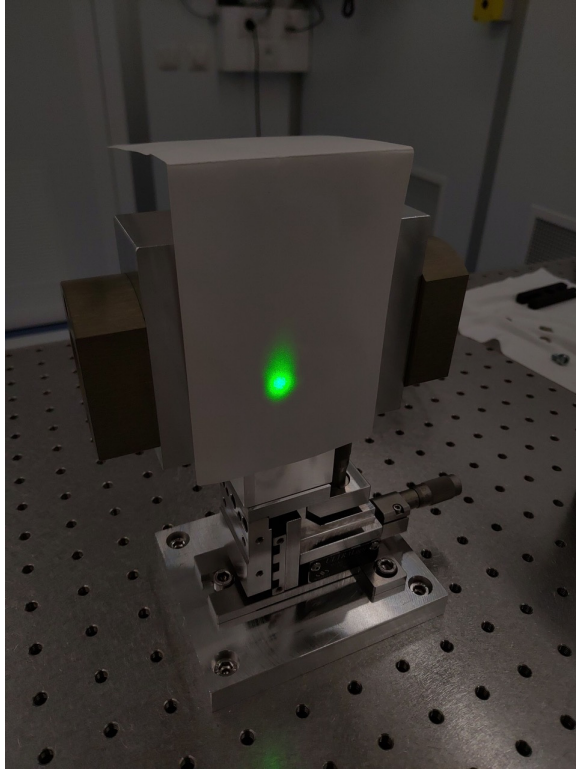


Fig. 18. Photo of initial alignment laser hitting its target after passing through the 240 m beam tube. Courtesy of Aaron Spector.

the first time. Stray light is currently being investigated before implementing the cavity before the wall as this allows us to couple a factor of 50 more power to the COB, making light leaks significantly easier to find. Nevertheless, the collaboration will use this opportunity to perform an initial science run at a reduced sensitivity without this cavity. Data taking for this run is expected to begin in February 2023.

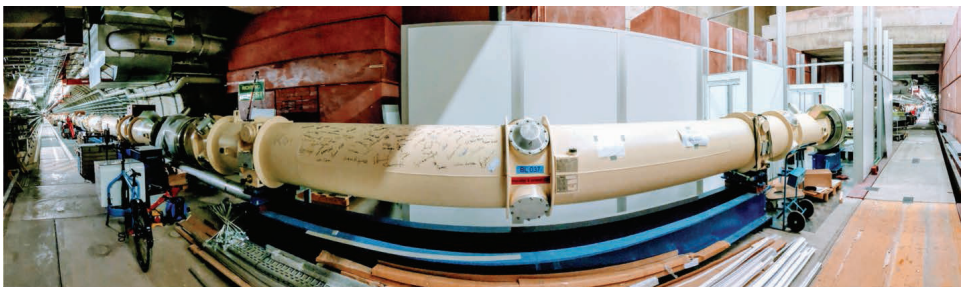


Fig. 19. Photo of the ALPS II magnet string. Courtesy of Aaron Spector.

5.3. Searching for the QCD axion with ARIADNE (Andrew A. Geraci)

The axion is a hypothetical particle that arises as a consequence of the PQ mechanism to solve the strong CP problem of QCD⁷¹ which is also well motivated as a dark matter candidate.¹³⁴ Axions can also mediate novel short-range spin-dependent interactions between fermions which are violating P and T symmetry.^{165–167} Depending on the model, monopole and dipole couplings, g_s and g_p , respectively, can occur for either electrons or nuclei. Although the couplings are extremely small for the interaction between single particles, a macroscopic object with $\sim 10^{23}$ atoms can produce a coherent field that can be detectable with a sensitive experiment.¹⁶⁸ Prior experimental tests of this interaction have been done with polarized gases,^{169–171,176} and in many cases combined laboratory measurements taken in parallel with astrophysical data have produced the most stringent constraints on the products of the coupling constants g_s and g_p .¹⁷³

The Axion Resonant InterAction DetectioN Experiment (ARIADNE) aims to detect axion-mediated interactions between an unpolarized source mass and a spin-polarized ^3He low-temperature gas.^{172,177} The potential of interest is given by $U_{sp}(r) = \frac{\hbar^2 g_s^N g_p^N}{8\pi m_f} \left(\frac{1}{r\lambda_a} + \frac{1}{r^2} \right) e^{-\frac{r}{\lambda_a}} (\hat{\sigma} \cdot \hat{r})$, where m_f is the mass of the fermion, $\hat{\sigma}$ is the Pauli spin matrix, \vec{r} is the vector between them and $\lambda_a = \hbar/m_A c$ is the axion Compton wavelength. For the QCD axion, the scalar and dipole coupling constants to nucleons, g_s^N and g_p^N , respectively, are correlated to the axion mass. Since it couples to $\hat{\sigma}$, which is proportional to the nuclear magnetic moment, the axion potential can be treated as generating a fictitious “magnetic field” B_{eff} . This fictitious field is used to resonantly drive spin precession in a laser-polarized cold ^3He gas. This is accomplished by spinning an unpolarized tungsten mass sprocket near the ^3He vessel. As the teeth of the sprocket pass by the sample at the nuclear Larmor precession frequency, the magnetization in the longitudinally polarized ^3He gas begins to precess about the axis of an applied field. This precessing transverse magnetization is detected with a SQUID. The ^3He sample acts as an amplifier to transduce the small fictitious magnetic field into a larger real magnetic field detectable by the SQUID. Assuming sources of systematic error and noise can be mitigated, the approach is expected to be spin-projection noise limited,¹⁷⁷ and in principle allows several orders of magnitude improvement, yielding sufficient sensitivity to detect the QCD axion (Fig. 1).

Several components of the experiment are undergoing fabrication and testing. Samples of hyperpolarized ^3He have been produced above a test cryostat using metastability exchange optical pumping,¹⁷⁵ with preliminary results of over 30 percent polarization on the few second timescale as shown in Fig. 2(a). We estimate that with improved external magnetic field homogeneity this can be improved by at least a factor of 2. Superconducting shielding is needed around the sample to screen it from ordinary magnetic field noise, which would otherwise limit the sensitivity of the measurement. Background magnetic field signals and noise are expected due to several mechanisms including Johnson noise, magnetic impurities and the magnetic

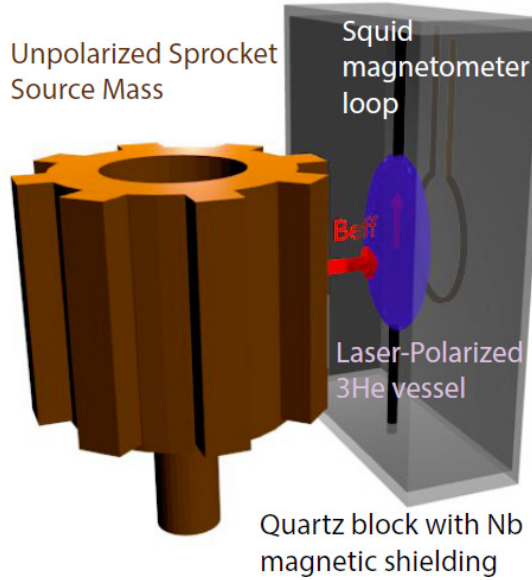


Fig. 20. Setup: A sprocket-shaped source mass is rotated so its “teeth” pass near a nuclear magnetic resonance sample at its resonant frequency. Courtesy of Andrew A. Geraci.

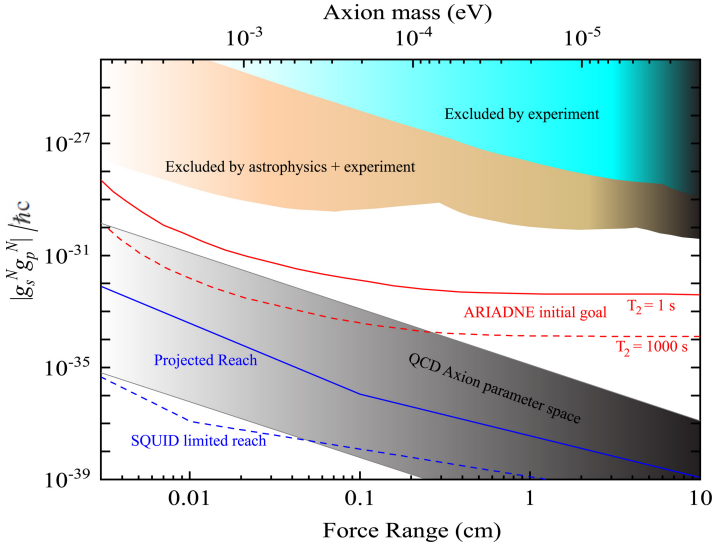
susceptibility of the tungsten sprocket. We have experimentally measured the magnetic noise in the sprocket¹⁸⁵ and verified that their level is such that the experiment can reach ultimate design sensitivity with a superconducting shielding factor of approximately 10^8 . Experimental tests suggest that such shielding factors can be achieved using a combination of thin film Nb and Pb foil shielding surrounding the quartz ^3He sample enclosure, as shown in Fig. 2(b).

Following its commissioning phase, the experiment will probe QCD axion masses in the higher end of the traditionally allowed axion window of $1\ \mu\text{eV}$ to $6\ \text{meV}$, which are not accessible by any existing experiment including dark matter haloscopes such as ADMX. Thus ARIADNE fills an important gap in the search for the QCD axion in this important region of parameter space. The experiment sources the axion in the lab, and can explore all mass ranges in our sensitivity band simultaneously, unlike experiments that must scan over the allowed axion oscillation frequencies (masses) by tuning a cavity or magnetic field.

When combined with other promising techniques,^{82,94,95,184,186} and existing experiments^{135,150,187} already at QCD axion sensitivity, ARIADNE could allow in principle the QCD axion to be searched for over its entire allowed mass range.

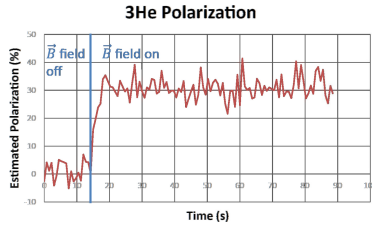
6. New Ideas and New Technologies

A comprehensive exploration of the allowed dark matter axion mass range at DFSZ sensitivity requires the development of new detection techniques and new technologies to enhance the sensitivity and mass reach of existing detectors. Of particular

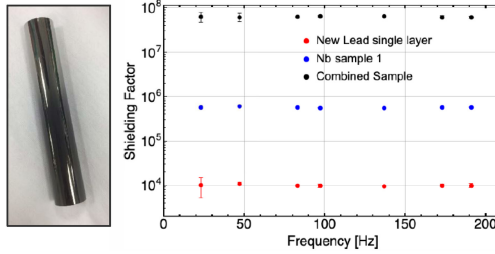


Source: Adapted from Refs. 177 and 171; courtesy of Andrew A. Geraci.

Fig. 21. (Color online) Projected reach for monopole-dipole axion mediated interactions. The band bounded by the red (dark) solid line and dashed line denotes the limit set by transverse magnetization noise, depending on achieved T_2 . Current constraints and expectations for the QCD axion also are shown.



(a)



(b)

Fig. 22. (a) Preliminary hyper-polarization results for ^3He above a test cryostat using metastability exchange optical pumping.¹⁷⁵ (b) Testing of magnetic shielding factor of sputtered thin film Nb and Pb foils applied to a quartz tube substrate. Courtesy of Andrew A. Geraci.

interest at this workshop were the use of quantum-sensing techniques involving state-squeezing and photon counting, along with increased magnet stored energy to enhance the sensitivity of axion haloscopes. Additional techniques using synthetic cavity resonances, quasiparticle interactions and broadband detectors were also discussed to probe axion masses outside the range accessible to current haloscopes.

6.1. Broadband axion searches with coaxial dish antennas
(Andrew Sonnenschein)

In a background of axion dark matter, a conducting surface becomes a source of electromagnetic radiation when there is a surface parallel magnetic field component. This nonresonant conversion mechanism is the basis of “dish antenna” axion search experiments.^{188,189} The available signal power in this type of experiment is orders of magnitude lower than in typical resonant cavity experiments such as ADMX with

$$P_{\text{signal}} = 8.3 \cdot 10^{-26} \text{ W} \cdot \left(\frac{A}{10 \text{ m}^2} \right) \left(\frac{B_{\parallel}}{10 \text{ Tesla}} \right)^2 \cdot \left(\frac{\rho_{\text{DM}}}{0.3 \text{ GeV/cm}^3} \right) \left(\frac{g_{a\gamma\gamma}}{3.92 \cdot 10^{-16} \text{ GeV}^{-1}} \right)^2 \left(\frac{1 \mu\text{eV}}{m_a} \right)^2.$$

Here, A is the surface area of the emitter, B_{\parallel} is the magnetic field component parallel to the surface, $g_{a\gamma\gamma}$ is the axion–photon coupling, m_a is the axion mass and ρ_{DM} is the local dark matter density. While the signal power of dish antenna experiments is very low, no tuning of the detector to match the axion mass is required and dish antennas can be scaled to large size with relative ease. Dish antennas are particularly appropriate for axions searches for masses above $20 \mu\text{eV}$, where it becomes increasingly impractical to build large-volume resonant cavity systems due to the small dimensions of the resonant structures.

Aside from the extremely low signal power, previously proposed experiments of this type suffer from difficulties related to the use of spherical or parabolic focusing elements, which are not well matched to the cylindrical geometry of solenoid magnets. Since solenoids are the easiest to engineer and most cost-effective type of large, high-field magnet, we propose instead to use the novel “coaxial dish reflector” geometry shown in Fig. 23. This design incorporates an axially symmetric inner reflector which focuses radially converging electromagnetic waves. As in a conventional reflecting optical system, the path lengths for all rays arriving at the focus are equal and the focus location is independent of wavelength. This geometry is particularly appropriate for experiments using subkelvin cryogenic sensors, where the dish and photosensor must both be cooled to achieve the highest possible sensitivity.

In Fig. 24, we illustrate the performance requirements for photosensors that would be needed to discover axions or ALPs in a system based on a solenoid with inner surface area 10 m^2 at a field of 10 Tesla (magnets of this scale are already available with existing technology). Discovery of axions with KSVZ- or DFSZ-level couplings requires sensors with noise-equivalent power or photon counting rates far

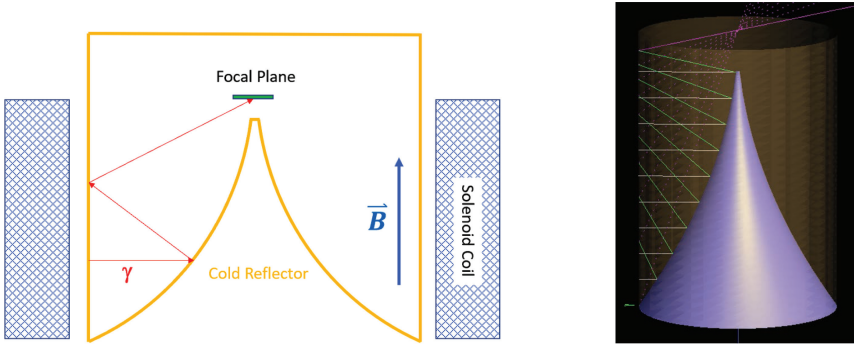


Fig. 23. Illustration of wideband axion detector concept. (Left) A parabolic surface of revolution is used to focus light rays emitted in the radial direction from a cylindrical emission surface inserted in the barrel of a solenoid magnet. The rays are focused near the tip of the inner reflector after two reflections. (Right) Ray trace of this optical geometry showing that all rays emitted along the barrel of the solenoid find a common focus. Courtesy of Andrew Sonnenschein.

below the current state of the art. The future development of sensors capable of photon counting at dark current rates below a few counts per day would enable axion discovery over a very wide frequency range. More details are given in a forthcoming publication.¹⁹⁰

This paper has been authored by Fermi Research Alliance, LLC under Contract No. DE-AC02-07CH11359 with the U.S. Department of Energy, Office of Science, Office of High Energy Physics.

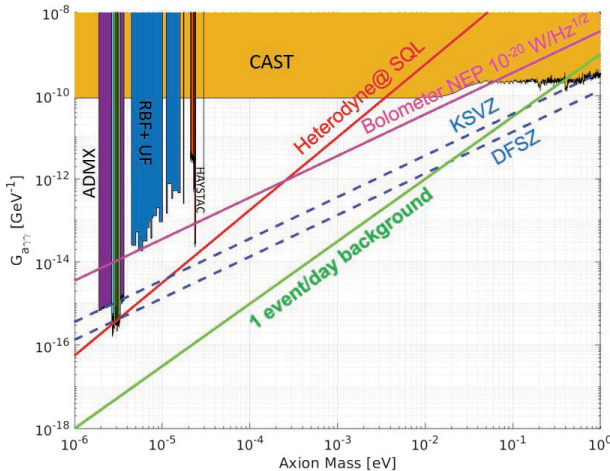


Fig. 24. Sensitivity of generic dish antenna experiments of three types: (1) heterodyne detection using a linear amplifier with noise temperature hf/K_B (the Standard Quantum Limit); (2) a bolometer experiment with noise-equivalent power of $10^{-20} \text{ W/Hz}^{1/2}$ and (3) a photon counting experiment with a dark count background of one event per day. In all cases, an emitter area of 10 m^2 , a magnetic field of 10 Tesla and an integration time of 100 days were assumed. Courtesy of Andrew Sonnenschein.

6.2. Axion quasiparticles for axion dark matter detection (David Marsh)

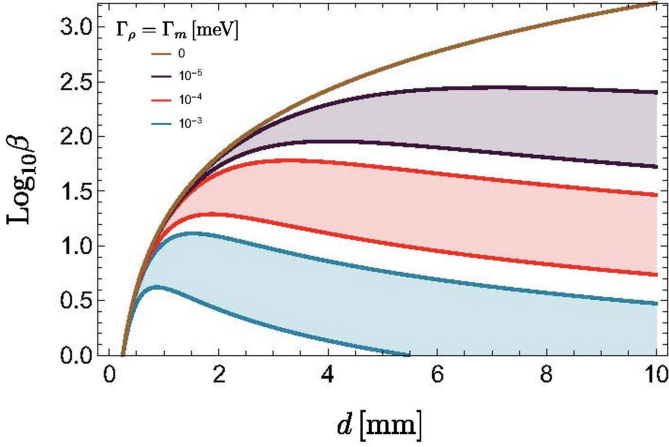
It has been suggested that certain antiferromagnetic topological insulators contain axion quasiparticles (AQs),²⁰⁴ and that such materials could be used to detect axion dark matter.^{178,205}

AQs have not been detected in experiments yet; however, several material candidates^{204,206} and search strategies²⁰⁴ have been suggested. One of the search strategies is to shine a THz source onto the AQ material candidate. The existence of AQs in the materials then leads to small transmission coefficients around the AQ mass, which can be measured using time domain spectroscopy as in other antiferromagnetic resonance measurements.²¹⁰ We have explicitly calculated the transmission coefficient by carefully taking into account the correct boundary conditions and modeling material losses. By comparing our calculations to future experiments one will be able to discover AQs. Furthermore, we show that after an AQ discovery the comparison of the measured transmission coefficient to our calculations enables one to fully characterize the AQ material parameters.

AQ materials can also be used to detect dark matter axions in the meV range. In addition to the original proposal in Ref. 205, we now present a more detailed calculation, which again takes into account the boundary conditions at the material surfaces as well as material losses. We further model the magnetic field dependence of the resonance assuming the AQ is a longitudinal, rather than transverse, antiferromagnetic excitation, which is consistent with theoretical expectations.^{194,206}

The topological Chern–Simons coupling between the AQ and the electromagnetic field causes the AQ to hybridize with the photon in the presence of an applied magnetic field, forming an axion–polariton with a mass-gap determined by the strength of the applied field. This mass gap causes the axion dark matter, AQ, and photon to resonantly mix and significantly enhances the dark matter induced photon signal. We use the boost factor β to describe how much the emitted photon signal is boosted in comparison to the signal that would be emitted by a dish antenna with the same cross-sectional area. In Fig. 25, we calculated the boost factor for different material losses with respect to the AQ material thickness d . The colored bands represent the variation of refractive index ranging from $n = 3$ to $n = 7$. Depending on the material losses, a boost factor β on the order of $10^{0.5} - 10^{2.5}$ can be reached. Losses lead to a skin depth, and correspondingly the boost factor is maximized at some optimal finite thickness, d . The optimal thickness lies in the mm range, where the exact value for the optimal thickness depends on the specific material losses.

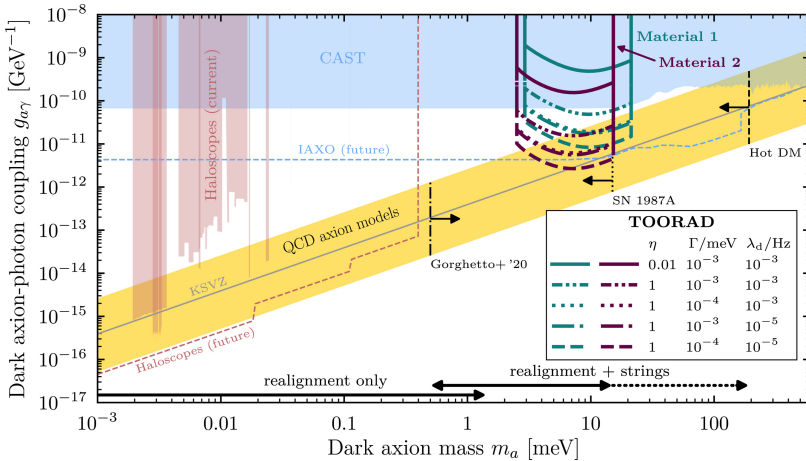
In Fig. 26, we show the projected sensitivity that could be reached by a scanning experiment with one layer of AQ material. Scanning different dark matter axion masses can be achieved by changing the strength of the strong external B -field that is applied parallel to the AQ material surface, which we assume varies in the range from 1 to 10 T. We assume a total scanning time of 3 years for every shown sensitivity curve, with each frequency scanned for an equal time. Sensitivity curves are shown for two different AQ material candidates. *Material 1* represents the predictions for



Source: From Ref. 178.

Fig. 25. Boost factor with respect to the AQ material thickness. The bands represent the refractive index varying from 3 to 7. The optimal thickness of the AQ materials lies in the mm regime.

$(\text{Bi}_{1-x}\text{Fe}_x)\text{Se}_2$, while *Material 2* stands for $\text{Mn}_2\text{Bi}_2\text{Te}_5$ as AQ material. The estimated losses vary between 10^{-3} and 10^{-4} meV. The photons that are emitted off the AQ material are detected with single-photon detection. We assume a coupling efficiency of $\eta = 1$ and dark count rates between 10^{-3} and 10^{-5} Hz, see for example Ref. 203. Our results demonstrate that AQ materials can probe a reasonable fraction of the QCD axion band (in yellow) in the mass range between 1 and 10 meV.



Source: From Ref. 178.

Fig. 26. Sensitivity forecast to the dark matter axions photon coupling $g_{a\gamma}$ with respect to the dark matter axions mass m_a . The forecasts are shown for two different AQ materials and various values for the material losses $\Gamma = \Gamma_m = \Gamma_\rho$ and single-photon detection dark count rates λ_d .

6.3. Searching for dark matter with a superconducting qubit (Akash Dixit)

Introduction

In this work, we demonstrate single-photon counting in the context of low-mass dark matter searches.²⁰⁰ We show an improvement of 15.7 dB over the quantum limit, leading to a 1300 times speed up of the search relative to a quantum limited amplifier.¹⁷⁹ We apply this novel detector to search for hidden photon dark matter, and are able to rule out candidates with kinetic mixing angle $\epsilon > 1.68 \times 10^{15}$ in a band around 6.011 GHz (24.86 μeV).

Photon counting with a qubit

We use a high-quality factor microwave cavity made of 99.9999% aluminum to accumulate the dark matter induced signal. We couple a superconducting qubit to the cavity to detect the presence of dark-matter-induced photons. The qubit cavity interaction is dispersive, the energy scale of the coupling is much smaller than the difference in energies of the qubit and cavity. In this limit, the interaction can be approximated as a product of the number operators, $H_{\text{int}}/\hbar = 2\chi a^\dagger a \frac{1}{2}\sigma_z$. When the interaction term is grouped with the qubit term, we see a cavity photon number-dependent shift of the qubit transition frequency, $H/\hbar = \omega_c a^\dagger a + \frac{1}{2} \times (\omega_q + 2\chi a^\dagger a)\sigma_z$. The strategy for photon detection is to monitor the qubit transition frequency using a Ramsey interferometry measurement to infer the cavity population.

Error mitigation

The main challenges to this protocol are measurement errors such as spurious qubit excitations, decay or readout errors. To reduce susceptibility to these false positives, we take advantage of the quantum nondemolition nature of the qubit–cavity interaction.^{180,181} Since the interaction is a product of the qubit and cavity number operators, measuring the cavity state does not destroy the state, but merely projects it on the Fock basis, which can be measured many times. We make 30 repeated measurements of the same photon and apply a hidden Markov-model-based analysis to reconstruct the initial cavity state and exponentially reduce the detector-based false positives, shown in Fig. 1. We find a residual population of background photons occupying the cavity with mean photon number 7.3×10^4 , corresponding to an effective temperature of 39.9 mK. Reducing this background is the next step in further increasing sensitivity to the extremely small signals expected from dark matter.

Hidden photon search

The detector is most sensitive to hidden photon dark matter candidates around the cavity frequency. Additionally, we are sensitive to regions periodically above and below the cavity frequency due to the nature of the interferometry measurement we conduct to count photons as seen in Fig. 2. We constrain the kinetic mixing angle $\epsilon \leq 1.68 \times 10^{15}$ around the cavity frequency of 6.011 GHz (24.86 μeV).

6.4. Resonant feedback (Ed Daw)

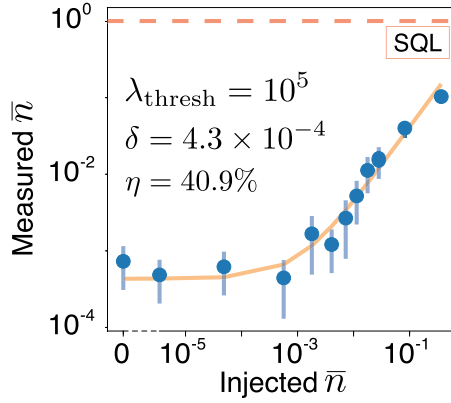
The idea of resonant feedback addresses several shortcomings of the usual ADMX-style resonant-cavity axion search. In the usual search, only the lowest transverse magnetic (TM) cavity mode has appreciable couplings to axions, and therefore the cavity must be mechanically tuned so that the lowest TM mode is at the putative axion frequency.^b These mechanical tuning systems introduce considerable complexity and heat loads. Furthermore, when the metallic tuning elements move through the magnetic field, considerable Faraday heating develops. The relative tuning bandwidth achieved with mechanical tuning is in the neighborhood of 15%. Searching in frequencies outside this bandwidth requires changing the cavity, tuning rods or cold radio frequency electronics, thus introducing considerable deadtime. The ideal form factor of the cavity E-field overlap with the magnetic field is around 0.4, considerably smaller than the form factor 1.0 of a uniform E-field aligned with a uniform B-field. Furthermore, the natural mass-scale of axions in a particular cavity axion search is set by the magnet-bore diameter. Moving the search to lower or higher masses in the same bore is challenging, the domain perhaps of “wire-in-cavity” searches or multicavity searches. Overall, the axion mass-range of a particular cavity search is relatively narrow, and broadening the range introduces considerable complexity.

Hence, should you favor extending axion mass (and frequency) beyond that of the usual QCD axion, a conventional cavity search will encounter severe technical challenges and would likely take a long time.

Some of these challenges are addressed with the idea of “resonant feedback”. Here, the idea is a resonance created via feedback, different from the intrinsic cavity resonance. This is an old idea for tuning radio electronics repurposed in axion searches. In slightly more detail, some of the oscillating electromagnetic signal far from an intrinsic cavity resonance is extracted from the cavity. The extracted signal is amplified and, with appropriate phasing and processing, introduced into the cavity. In effect, the external feedback circuit imposes new resonant boundary conditions on the cavity, where the resonant conditions are controlled parametrically by external electronics. In particular, the frequencies of the resonances can be adjusted — and there may be many such resonances — as well as the Q for each.

This idea has a number of advantages. There can be many such simultaneous resonances. The resonant frequencies are no longer set by the magnet-bore diameter and can in principle cover a very broad frequency range. The mechanical tuning mechanism with its tuning rods is then used to shift the cavity intrinsic resonances to fill in the search at frequencies of the cavity intrinsic resonances; this is fine-tuning as opposed to the gross-tuning in the usual cavity search and is considerably less complicated. The quality factor Q of each mode is likewise parametrically controllable, which allows the Q to optimally match the putative axion lineshape.

^bIn principle, the resonant frequency could be tuned nonmechanically with an electrically adjustable reactance loading the cavity, but this idea has not yet transitioned from R&D to a production experiment.



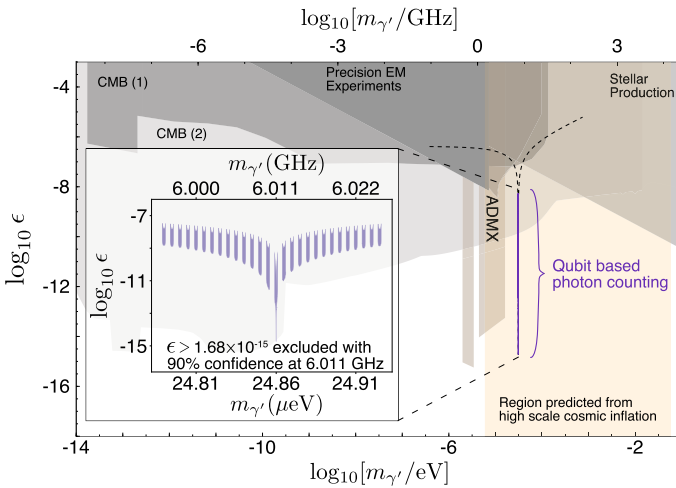
Source: From Ref. 200.

Fig. 27. Counting photons with a qubit. Injected photons are counted using 30 repeated parity measurements with an efficiency of $\eta = 40.9\%$. The false positive probability, δ , is dominated by background photons.

The electromagnetic structure within the bore can be more like that of a parallel-plate capacitor with a near-unity form factor.

The challenge of this idea is to be able to extract electromagnetic power from the cavity, process the signal and inject it into the cavity while keeping the noise ultra-low.

As a demonstration of this idea, a team from Sheffield University and the University of Washington introduced such a system to the “sidecar” ADMX cavity



Source: From Ref. 200.

Fig. 28. Hidden photon exclusion. Large regions of dark matter parameter space can be searched using qubit-based photon counting.

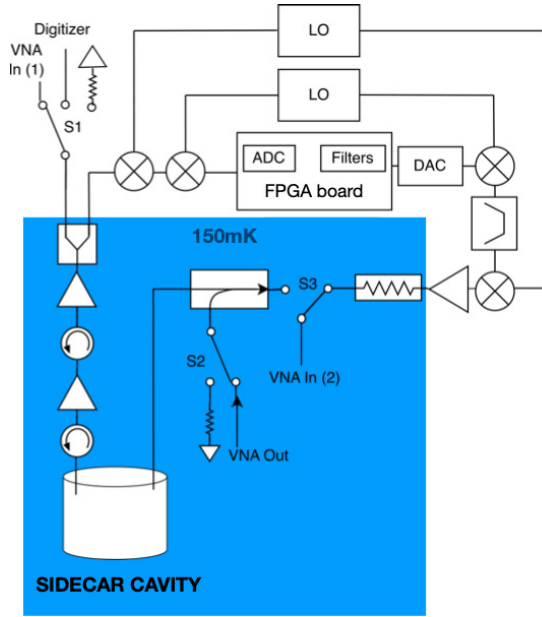


Fig. 29. Resonant feedback block diagram. Courtesy Edward Daw.

in operation during normal data-taking (system cold and magnetic field on). The block diagram of the system is shown in Fig. 29. This system introduces narrow-band resonances on top of the TM_{010} mode of the sidecar cavity containing one tuning rod. This intrinsic cavity mode has resonant frequency around 5 GHz and Q around 20,000. The electric field of the cavity mode is critically coupled to the input of a low-noise amplifier chain, which in turn feeds a superheterodyne receiver, with local oscillators at 10.7 MHz and 200 kHz. The output of the mix-down stage is then digitized by an on-board 490 kHz sampling-rate ADC on a field programmable gate array (FPGA). The analog-to-digital converter (ADC) output is then filtered using a digital resonant filter, then re-converted to analog. The analog signal is then mixed-up back to the carrier frequency.

Looking at the block diagram, with S3 open, a network analyzer measures the open-loop gain; the gain is set near 0 dB (unity gain) relative to the resonant peak induced in the FPGA digital electronics. With S3 closed, the processed signal is injected into the cavity, thereby closing a feedback loop. In this closed loop, fixed-frequency signals are injected into the cavity, while a conventional receiver acquires cavity power spectra in the neighborhood of the single digitally induced resonance.

Figure 30 shows swept power for five different induced narrow-band frequencies with Q near 10^7 on top of the broad intrinsic TM_{010} cavity resonance at 4.9 GHz with Q near 20,000. All five frequencies were injected at the same power, and you can observe the developed receiver power is enhanced near the induced resonances in the same manner as for the intrinsic cavity resonance.

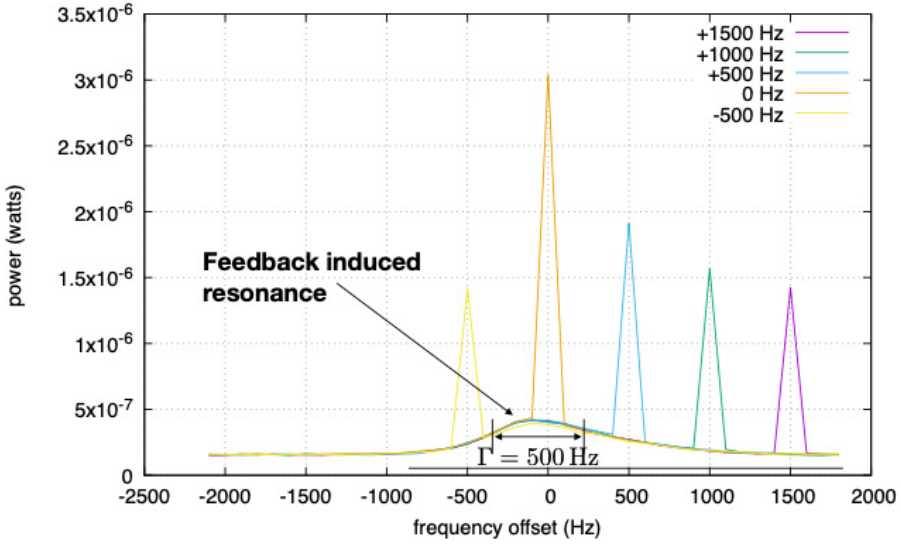


Fig. 30. Swept power for five different induced narrow-band frequencies with Q near 10^7 on top of the broad intrinsic TM_{010} cavity resonance at 4.9 GHz with Q near 20 k. Courtesy Edward Daw.

The current state of this idea is as follows. Inducing resonances in an electromagnetic structure is demonstrated in a cavity search. These resonances had Q s near 10^7 , somewhat higher than optimal for the expected lineshape of a virtualized halo axion. The corresponding developed cavity power was enhanced as expected for the Q . Interestingly, the test system was an ADMX cavity during normal data-taking (cold and magnetic field on), so these test data are in principle sensitive to axions.

The near-term development of this idea includes the following. Demonstrate that the induced Q can be reduced to optimal. Automate the setting of the open-loop gain to stabilize it near 1 (0 dB) and the loop phase shifts at integer multiples of 2π . Introduce multiple resonances simultaneously. Characterize the shape of the induced resonances and ensure they match the model of a cavity resonance feeding the reactance of the output transmission line and loads.

The advocates of this idea hope this can be deployed on a production search in the next year. This is a promising approach to speeding up and expanding the mass-reach of cavity axion searches.

6.5. High-temperature superconductor magnets for axion dark matter searches (Yannis K. Semertzidis)

The axion search sensitivity scales with the magnetic field applied in the axion-to-photon conversion region and the frequency scanning speed goes with its fourth power. High field magnets are especially needed in the high-frequency axion search requiring resonators with 100–20 mm aperture suitable for about 2–10 GHz range. Recently, there are several ideas proposed that can be used to probe high-frequency

axions beyond the “natural” size of the magnet aperture,^{93,135} but with a maximum scaling factor of about 3 or 4. Even more recent ideas could provide a larger frequency enhancement factor^{144,182} but these ideas have not produced any significant sensitivity in axion dark matter search.

Magnets made solely out of copper can have a large volume and reasonable field, but running them for a significant time is not affordable due to immense ohmic losses. On the other hand, superconducting magnets have two important limitations in achieving high magnetic fields. First, their critical current density depends on the magnetic field value, meaning that magnets made of the common superconducting cable of NbTi have a maximum useful field of about 9 T, those made of Nb₃Sn can go up to 15–20 T, whereas those made out of high-temperature superconductors (HTS) could theoretically go up to 100 T. Second, the hoop stresses due to Lorentz forces are large, especially at the ends of a solenoid magnet. This means, that once a successful magnet design with a certain aperture is established, it can theoretically be made very long to achieve high volume and thus a large energy content, proportional to B^2V . At Brookhaven National Laboratory (BNL), the no-insulation, single layer conservative geometry was adopted,^{191,192} with 50 μm Hastelloy for rigidity and 20 μm Cu for electrical stability, providing 50% margin in both critical current and hoop forces. It would be advantageous to make the magnet long to provide B^2V twice or even more than the originally intended one, at the cost of the extra material and labor. Peeling issues that have been observed in other HTS magnets¹⁹³ are avoided by paying special attention to the issue. Repeated induced quenches with both excessive currents and heat on the coils indicated no damage accumulation.

HTS can sustain high B-fields of order 100 T before the critical current density collapses, as is the case with ordinary superconductors, and they are the only choice we are left with when high field magnets are required. With the BNL Magnet Division, we have developed a project with a goal to reach 25 T in a bore aperture of 100 mm using second generation, no-insulator HTS tapes. A total of 28 coils were required to finish the project, but it was stopped by forces beyond our control when 16 coils were manufactured and successfully tested. This project is ready and should be restarted to finish the magnet, perhaps even making it longer to make up for the lost time.

We acknowledge IBS of the Republic of Korea (project system code: IBS-R017-D1-a00).

6.6. An overview of high field HTS solenoid technology (Mark D. Bird)

Performance of an axion detector is governed largely by the square of the magnetic field integrated over the volume of the resonator, which is frequently approximated as the square of the central field multiplied by the volume of the resonator: B_0^2V . If the goal is to maximize B_0^2V , the fusion community is building large-bore, high field magnets such as ITER CS ($\sim 12,000 \text{ T}^2\text{m}^3$), but these have bores a few meters in diameters and would require large resonators, which are typically seen as not being

practical. If the goal is to get higher B_0^2V than the existing ADMX with modest cost, securing an ultra-high field MRI magnet would be a good step. ADMX is now pursuing a 9.4T MRI magnet built by Magnex/GE and owned by the University of Illinois at Chicago. This will provide a significant step forward. The highest field magnets worldwide (>30 T) have $B_0^2V < 11\text{T}^2\text{m}^3$. MRI magnets have $B_0^2V > 100\text{T}^2\text{m}^3$. To minimize cost, one should build the largest resonator one can plus the highest field magnet one can with bore large enough for the resonator to fit.

For axion detection, extended periods of time (months) at field are required. Direct current magnets are required and the cost of electricity for a resistive magnet is prohibitive. Superconducting magnets are traditionally built from the low-temperature superconductors, NbTi and Nb₃Sn, which are limited to magnetic fields < 25 T.

If higher field is required, the HTS (REBCO, Bi-2212 and Bi-2223) are now enabling higher field magnets to be realized. The National High Magnetic Field Laboratory in Tallahassee, Florida, now has the highest field superconducting magnet in the world operating at 32 T and has initiated development of a 40 T magnet. There are numerous subtleties associated with realizing magnets at these extreme fields, including the effects of screening currents, quench management and the reproducibility and uniformity of the commercial conductors.

6.7. *Enhancing axion detection with quantum squeezing (K. M. Backes for the HAYSTAC collaboration)*

HAYSTAC (Haloscope at Yale Sensitive to Axion Cold dark matter) is a specific realization of the axion haloscope concept,⁶⁰ which searches for axions through the coupling $g_{a\gamma\gamma}$ of the hypothetical axion field a to $\mathbf{E} \cdot \mathbf{B}$ through the interaction,

$$\mathcal{L} \sim g_{a\gamma\gamma} a \mathbf{E} \cdot \mathbf{B}. \tag{4}$$

A traditional haloscope is composed of a tunable microwave cavity in a large magnetic field \mathbf{B} . An antenna is inserted into the cavity to extract axion-sensitive voltage fluctuations and send them to a low-noise amplifier. At the output, the axion would present as a narrowband excised of power emerging from the cavity at a frequency proportional to the axion mass, $\nu_a = m_a c^2/h$, which is resonantly enhanced when that frequency falls within the cavity bandwidth.

In order to search for axions within a range of potential masses, we step the resonance of the microwave cavity through frequency space at a rate R (in Hz/s). For a haloscope using a linear amplification scheme, R is fundamentally limited by the zero-point fluctuations of the cavity mode,¹⁹⁴ which create a noise floor that can only be overcome using quantum-enhanced measurement techniques.¹⁸³

HAYSTAC has implemented one such quantum-enhanced measurement technique, by coupling the cavity to a squeezed state receiver composed of two flux-pumped Josephson parametric amplifiers (JPAs).^{194,208} In the full HAYSTAC system, we demonstrate 4.0 dB of off-resonant vacuum squeezing as measured at the detector output, corresponding to a factor of 1.9 scan-rate enhancement.

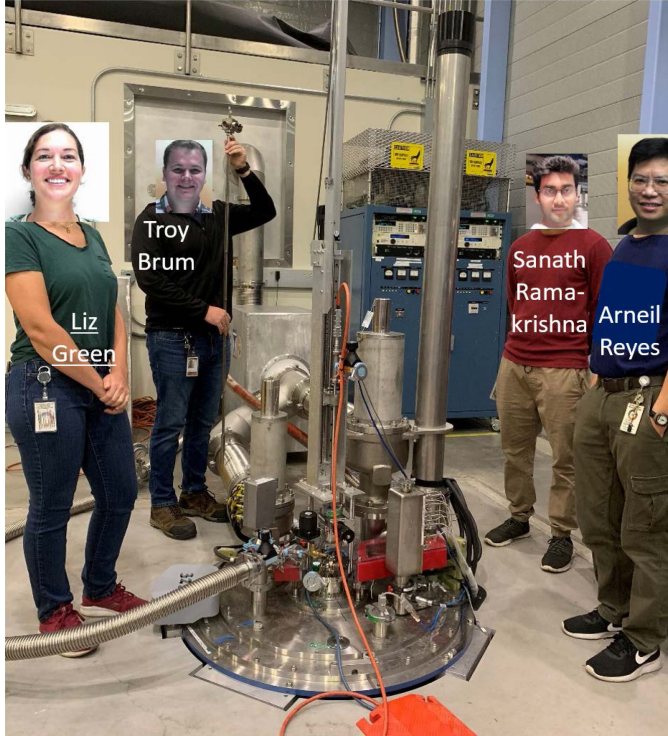


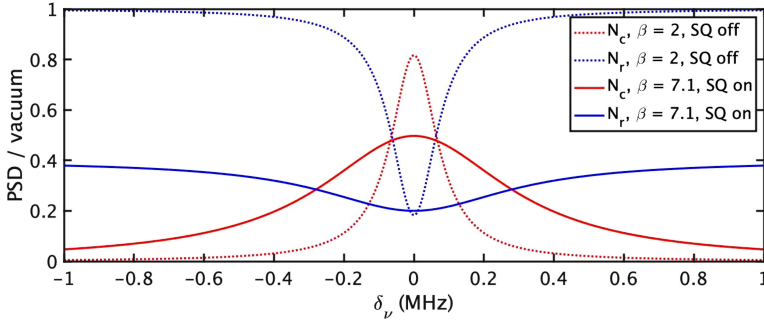
Fig. 31. The first users of the 32 T superconducting magnet. Courtesy of Mark Bird.

The cavity obeys the Hamiltonian

$$\hat{H} = \frac{h\nu_c}{2}(\hat{X}^2 + \hat{Y}^2), \quad (5)$$

where \hat{X} and \hat{Y} quadratures obey the commutation relation $[\hat{X}, \hat{Y}] = i$. The first JPA, the squeezer, squeezes the vacuum state at its input, reducing the \hat{X} quadrature variance below vacuum and amplifying the \hat{Y} quadrature accordingly.^{179,207} This state is guided into the cavity where the axion field would displace the squeezed state. The squeezed quadrature (\hat{X}) is then near-noislessly amplified by the second JPA, the amplifier.

Squeezing increases R by improving the bandwidth over which the detector is sensitive to axions at each tuning step. Widening the cavity bandwidth allows for larger frequency tuning steps, which allows the cavity to be tuned through frequency space more quickly. In the absence of squeezing, the tradeoff of going to a higher bandwidth means we need to integrate disproportionately longer at each frequency, making an axion search take longer. Squeezing provides a way to increase the bandwidth without paying that sensitivity penalty. This benefit is represented in Fig. 32. Red shows noise originating in the cavity (N_c), which is where the axion would manifest, and blue is noise that is generated at the temperature of the fridge



Source: From Ref. 202.

Fig. 32. (Color online) Theoretical noise curves for the ideal squeezing (solid lines) and no squeezing (dotted lines) cases. Each curve shows the power spectral density of Johnson–Nyquist noise normalized to the vacuum value. Noise reflected off of the cavity (N_r) is shown in blue, and noise originating within the cavity (N_c) is shown in red. Squeezing reduces the reflected noise and allows the coupling of the receiver to the cavity (β) to be increased without paying a sensitivity penalty.

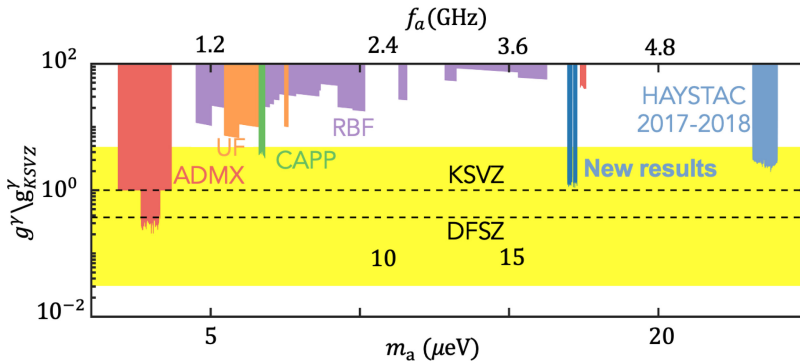


Fig. 33. (Color online) Axion haloscope exclusions from Ref. 202. HAYSTAC’s recent results²⁰² are shown here with the results from other axion haloscopes (see Ref. 209). The band representing QCD axion models²⁰¹ is shown in yellow. The KSVZ^{134,195} and DFSZ^{88,197} models are shown as dashed black lines.

and reflects off of the cavity (N_r). In the no-squeezing case, N_c is only dominant over a small bandwidth. Squeezing N_r increases the range over which N_c is dominant and allows us to increase our bandwidth by increasing the coupling of the solid-state relay to the cavity (β).

At the output of the solid-state relay, we collect axion-sensitive voltage fluctuations in the \hat{X} quadrature and analyze these fluctuations as described in Refs. 202, 196 and 198. Over the course of approximately 100 days, we probed over 70 MHz of well-motivated parameter space.^{12,199} With these data, we place a constraint on the axion mass m_a within the 16.96–17.12 and 17.14–17.28 $\sim \mu\text{eV}/c^2$ windows at a coupling of $g_\gamma \geq 1.38 \times g_\gamma^{\text{KSVZ}}$ at 90% confidence (Fig. 33). These results mark the first time that an axion search has been enhanced with quantum squeezing.

7. Conclusion

Axion science is a rapidly moving field, and new developments in theory, cosmology, astrophysics and experiment continue to appear at a rapid clip. As a result, the topics covered in these proceedings cover a broad but necessarily incomplete overview of current research at the time the workshop took place. With apologies to those who were omitted due to lack of time and space, we can now give partial answers to the driving questions of the workshop.

With respect to the theory of QCD axions, it seems that axions in the 1–1000 μeV range, with the benchmark couplings down to DFSZ, are still the best motivated from the simplest theories. However, it is clear that more sophisticated models may allow or favor masses far below and above this range, and these models should continue to be investigated.

Regarding the distribution of axion dark matter, the simplest galactic Structure Formation models predict a smooth distribution of dark matter in our local space with a density in the $\rho_{\text{DM}} \simeq 0.3 - 0.5 \text{ GeV cm}^{-3}$ range.²⁵ However, certain theories predict significant dark-matter substructure, and this substructure could drastically change the signal developed in experimental axion searches. Future experiments should consider ways of being sensitive to transient signals, in addition to the traditional time invariant signals, which may be a feature of these new models with substructure. It has also come to light that interactions of axions with astrophysical objects such as black holes could lead to new avenues for potential detection, particularly in gravity waves detected by LIGO and other gravity-wave detectors.

In the past decade, a number of experimental techniques have arisen that probe nuclear axion couplings. These experiments are making exciting progress, but much work needs to be done to reach the predicted QCD axion couplings at expected dark matter densities. Furthermore, unlike the experiments that rely on the axion–photon coupling, the axion–nucleon coupling introduces considerably more model dependence.

The axion haloscope, probing the axion–photon coupling, is at present still the only technique that can explore the most theoretically well-motivated axion dark matter masses and couplings. Yet only a small fraction of this parameter space has yet been explored and there is a clear need for improvements in experiments to allow a discovery to happen in a timely manner. Fortunately, as demonstrated in this workshop, there are promising directions for haloscopes designs beyond the current generation.

In addition to the searches for dark matter axions there are also methods to directly measure axions produced from strong photon fields, either in the laboratory in lasers or from astrophysical sources such as the sun. Such techniques suffer from the challenge arising from the requirement to both produce the axions and then reconvert them into photons for detection, which requires a $(g_{a\gamma\gamma})^4$ rather than $(g_{a\gamma\gamma})^2$ for axion detection. The advantage of these techniques is that uncertainties in the local dark matter density are removed. Upcoming experiments such as ALPS-II and BabyIAXO will explore some interesting axion models with stronger couplings than the QCD axion independently of their contribution to dark matter.

Beyond the axion–photon coupling, new complimentary experiments are being developed to probe dark matter axions couplings to either electrons or nuclei such as QUAX and CASPER, respectively. Other techniques include looking for the axion to serve as a new field which would be a force mediator for interactions at short distances (i.e. “Fifth Force” searches). The ARIADNE experiment is an example of these searches but new ideas are additionally being discussed.

As mentioned, enhancing the ability of an axion haloscope to probe a larger range of axion masses at QCD sensitivity is a key path to discovery. There are three approaches being taken to move this technique forward.

The first of these approaches is improvements in magnet technology, in which advancements in High Temperature Superconductors driven by fusion research point a way to constructing new, very large field and large volume magnets. This includes systems up to, say, 32 T and development of potential 40 T magnet systems.

Another approach is to enhance haloscopes with more sophisticated resonator design. Improvements on cavity tunability, quality factor and effective detector volume (i.e. the number of multiplexed resonators) are needed to increase sensitivity and widen the axion mass reach. New broadband or semi-broadband techniques that rely on focusing axions produced from mirror surfaces in a magnetic field, such as proposed by the BREAD and MADMAX experiments could provide an alternative to relying on the resonance techniques by trading sensitivity for resonator simplicity.

Finally, the implementation of quantum sensing techniques to reduce background noise will likely be needed to increase the scan rate of haloscope searches. While thermal noise can be reduced with dilution refrigerators and amplifier noise with sophisticated amplifiers, there is a remaining noise contribution, known as the Standard Quantum Limit (SQL), that limits linear amplifier noise performance. Qubit-based photon counting and squeezing techniques will likely play a role in evading the SQL in future quantum-enhanced axion searches, thereby greatly improving experiment sensitivity.

It is worth noting that there is likely no one ONE improvement that can single-handedly achieve QCD sensitivity in the 20–1000 μeV range. In other words, just a large magnetic field, just the use of multiple cavities, just the use of superconducting cavities, or just the implementation of novel noise-reducing quantum sensing techniques will be insufficient for covering the entire well-motivated axion mass window at DFSZ sensitivity. These individual enhancements, when proven to work in isolation, must then be made to work in concert in a production experiment. Furthermore, as detector designs evolve to address sensitivity challenges, they inherently become more complicated. Tools must be developed to allow high duty-factor operation of detectors with more interconnected resonant mode structures and moving parts. The next decade will prove to be an exciting time as new, well-developed multicavity systems begin to probe further into plausible dark matter space and exciting new techniques work their way through the R&D stages and are deployed in fully fledged experiments. As a result we are certainly closer to discovering (or ruling out) the dark matter axion than ever before.

Acknowledgments

The proceedings' editors gratefully acknowledge the generous workshop support from the Heising-Simons Foundation under Grant ID 2019-1615 to the University of Washington. We also acknowledge support from the U.S. Department of Energy under contract numbers DE-SC0011665 (University of Washington), DE-SC0009800, (University of Washington), and under the auspices of the U.S. Department of Energy by Lawrence Livermore National Laboratory under Contract DE-AC52-07NA27344. LLNL document release number: LLNL-PROC-850173. Pacific Northwest National Laboratory is a multi-program national laboratory operated for the U.S. DOE by Battelle Memorial Institute under Contract No. DE-AC05-76RL01830. PNNL document release number: PNNL-SA-186615.

ORCID

Christian Boutan  <https://orcid.org/0000-0002-1470-1946>
Gianpaolo Carosi  <https://orcid.org/0000-0003-0130-6979>
Leslie J Rosenberg  <https://orcid.org/0000-0003-0686-0485>
Gray Rybka  <https://orcid.org/0000-0001-9973-1564>
K. M. Backes  <https://orcid.org/0000-0001-7134-946X>
Chelsea Bartram  <https://orcid.org/0000-0002-7468-5992>
Masha Baryakhtar  <https://orcid.org/0000-0002-7631-2604>
Mark D. Bird  <https://orcid.org/0000-0001-9617-2875>
Caterina Braggio  <https://orcid.org/0000-0001-7563-4970>
Dmitry Budker  <https://orcid.org/0000-0002-7356-4814>
Raymond T. Co  <https://orcid.org/0000-0002-8395-7056>
Edward Daw  <https://orcid.org/0000-0002-3780-5430>
Akash Dixit  <https://orcid.org/0000-0001-6699-7198>
Andrew A. Geraci  <https://orcid.org/0000-0001-7009-0118>
Chang Lee  <https://orcid.org/0000-0002-1605-2273>
Soohyung Lee  <https://orcid.org/0000-0001-5959-9407>
David Marsh  <https://orcid.org/0000-0002-4690-3016>
Ciaran O'Hare  <https://orcid.org/0000-0003-3803-9384>
Ken'ichi Saikawa  <https://orcid.org/0000-0002-9205-9813>
Chiara P. Salemi  <https://orcid.org/0000-0002-7429-6612>
Yannis K. Semertzidis  <https://orcid.org/0000-0001-7941-6639>
Andrew Sonnenschein  <https://orcid.org/0000-0002-3280-5300>
Aaron Spector  <https://orcid.org/0000-0002-6575-8192>
Michael E. Tobar  <https://orcid.org/0000-0002-3139-1994>
Julia Vogel  <https://orcid.org/0000-0002-5850-5517>
Ariel Zhitnitsky  <https://orcid.org/0000-0002-2049-228X>

References

1. R. T. Co, L. J. Hall and K. Harigaya, *Phys. Rev. Lett.* **124**, 251802 (2020), arXiv:1910.14152 [hep-ph], doi:10.1103/PhysRevLett.124.251802.
2. R. T. Co, L. J. Hall, K. Harigaya, K. A. Olive and S. Verner, *J. Cosmol. Astropart. Phys.* **2020**, 036 (2020).
3. J. Preskill, M. B. Wise and F. Wilczek, *Phys. Lett. B* **120**, 127 (1983), doi:10.1016/0370-2693(83)90637-8.
4. L. Abbott and P. Sikivie, *Phys. Lett. B* **120**, 133 (1983), doi:10.1016/0370-2693(83)90638-X.
5. M. Dine and W. Fischler, *Phys. Lett. B* **120**, 137 (1983), doi:https://doi.org/10.1016/0370-2693(83)90639-1.
6. R. T. Co, L. J. Hall and K. Harigaya, *J. High Energy Phys.* **1**, 172 (2021), arXiv:2006.04809 [hep-ph], doi:10.1007/JHEP01(2021)172.
7. R. T. Co and K. Harigaya, *Phys. Rev. Lett.* **124**, 111602 (2020), arXiv:1910.02080 [hep-ph], doi:10.1103/PhysRevLett.124.111602.
8. R. T. Co, N. Fernandez, A. Ghalsasi, L. J. Hall and K. Harigaya, *J. High Energy Phys.* **3**, 017 (2021), arXiv:2006.05687 [hep-ph], doi:10.1007/JHEP03(2021)017.
9. L. Abbott and P. Sikivie, *Phys. Lett. B* **120**, 133 (1983), doi:https://doi.org/10.1016/0370-2693(83)90638-X.
10. R. L. Davis, *Phys. Lett. B* **180**, 225 (1986), doi:10.1016/0370-2693(86)90300-X.
11. M. Kawasaki, K. Saikawa and T. Sekiguchi, *Phys. Rev. D* **91**, 065014 (2015), doi:10.1103/PhysRevD.91.065014.
12. V. B. Klaer and G. D. Moore, *J. Cosmol. Astropart. Phys.* **2017**, 049 (2017), arXiv:1708.07521 [hep-ph], doi:10.1088/1475-7516/2017/11/049.
13. M. Gorghetto, E. Hardy and G. Villadoro, *J. High Energy Phys.* **2018**, 151 (2018), arXiv:1806.04677 [hep-ph], doi:10.1007/JHEP07(2018)151.
14. M. Buschmann, J. W. Foster, A. Hook, A. Peterson, D. E. Willcox, W. Zhang and B. R. Safdi, *Nat. Commun.* **13**, 1049 (2022), arXiv:2108.05368 [hep-ph], doi:10.1038/s41467-022-28669-y.
15. A. Vaquero, K. S. J. Redondo, and J. Stadler, *J. Cosmol. Astropart. Phys.* **2019**, 012 (2019).
16. A. R. Zhitnitsky, *J. Cosmol. Astropart. Phys.* **2003**, 010 (2003), doi:10.1088/1475-7516/2003/10/010.
17. A. Zhitnitsky, *Mod. Phys. Lett. A* **36**, 2130017 (2021), https://doi.org/10.1142/S0217732321300172, doi:10.1142/S0217732321300172.
18. H. Fischer, X. Liang, A. Zhitnitsky, Y. Semertzidis and K. Zioutas, *Phys. Rev. D* **98**, 043013 (2018), doi:10.1103/PhysRevD.98.043013.
19. D. Budker, V. V. Flambaum, X. Liang and A. Zhitnitsky, *Phys. Rev. D* **101**, 043012 (2020), doi:10.1103/PhysRevD.101.043012.
20. J. W. Foster, N. L. Rodd and B. R. Safdi, *Phys. Rev. D* **97**, 123006 (2018), arXiv:1711.10489 [astro-ph.CO], doi:10.1103/PhysRevD.97.123006.
21. C. A. J. O'Hare and A. M. Green, *Phys. Rev. D* **95**, 063017 (2017), arXiv:1701.03118 [astro-ph.CO], doi:10.1103/PhysRevD.95.063017.
22. S. Knirck, A. J. Millar, C. A. J. O'Hare, J. Redondo and F. D. Steffen, *J. Cosmol. Astropart. Phys.* **2018**, 051 (2018), doi:10.1088/1475-7516/2018/11/051.
23. D. F. J. Kimball *et al.*, Overview of the Cosmic Axion Spin Precession Experiment (CASPER), in *Microwave Cavities and Detectors for Axion Research*, *Springer Proceedings in Physics*, eds. G. Carosi, G. Rybka, Vol. 245 (Springer, Cham, 2020), pp. 105–121, https://doi.org/10.1007/978-3-030-43761-9_13.

24. A. Garcon, J. W. Blanchard, G. P. Centers, N. L. Figueroa, P. W. Graham, D. F. Jackson Kimball, S. Rajendran, A. O. Sushkov, Y. V. Stadnik, A. Wickenbrock, T. Wu and D. Budker, *Sci. Adv.* **5** (2019), <https://advances.sciencemag.org/content/5/10/eaax4539.full.pdf>, doi:10.1126/sciadv.aax4539.
25. P. F. de Salas and A. Widmark, *Rep. Prog. Phys.* **84**, 104901 (2021), doi:10.1088/1361-6633/ac24e7.
26. A. G. A. Brown, A. Vallenari, T. Prusti, J. H. J. de Bruijne, C. Babusiaux, C. A. L. Bailer-Jones, M. Biermann, D. W. Evans, L. Eyer, F. Jansen, C. Jordi, S. A. Klioner, U. Lammers, L. Lindegren, X. Luri, F. Mignard, C. Panem, D. Pourbaix, S. Randich, P. Sartoretti, H. I. Siddiqui, C. Soubiran, F. van Leeuwen, N. A. Walton, F. Arenou, U. Bastian, M. Cropper, R. Drimmel, D. Katz, M. G. Lattanzi, J. Bakker, C. Cacciari, J. Castañeda, L. Chaoul, N. Cheek, F. De Angeli, C. Fabricius, R. Guerra, B. Holl, E. Masana, R. Messineo, N. Mowlavi, K. Nienartowicz, P. Panuzzo, J. Portell, M. Riello, G. M. Seabroke, P. Tanga, F. Thévenin, G. Gracia-Abril, G. Comoretto, M. Garcia-Reinaldos, D. Teyssier, M. Altmann, R. Andrae, M. Audard, I. Bellas-Velidis, K. Benson, J. Berthier, R. Blomme, P. Burgess, G. Busso, B. Carry, A. Cellino, G. Clementini, M. Clotet, O. Creevey, M. Davidson, J. De Ridder, L. Delchambre, A. Dell’Oro, C. Ducourant, J. Fernández-Hernández, M. Fouesneau, Y. Frémat, L. Galluccio, M. García-Torres, J. González-Núñez, J. J. González-Vidal, E. Gosset, L. P. Guy, J.-L. Halbwachs, N. C. Hambly, D. L. Harrison, J. Hernández, D. Hestroffer, S. T. Hodgkin, A. Hutton, G. Jasniewicz, A. Jean-Antoine-Piccolo, S. Jordan, A. J. Korn, A. Krone-Martins, A. C. Lanzafame, T. Lebzelter, W. Löffler, M. Manteiga, P. M. Marrese, J. M. Martín-Fleitas, A. Moitinho, A. Mora, K. Muinonen, J. Osinde, E. Pancino, T. Pauwels, J.-M. Petit, A. Recio-Blanco, P. J. Richards, L. Rimoldini, A. C. Robin, L. M. Sarro, C. Siopis, M. Smith, A. Sozzetti, M. Süveges, J. Torra, W. van Reeve, U. Abbas, A. Abreu Aramburu, S. Accart, C. Aerts, G. Altavilla, M. A. Álvarez, R. Alvarez, J. Alves, R. I. Anderson, A. H. Andrei, E. Anglada Varela, E. Antiche, T. Antoja, B. Arcay, T. L. Astraatmadja, N. Bach, S. G. Baker and Balaguer-Nú, *Astron. Astrophys.* **616**, A1 (2018), doi:10.1051/0004-6361/201833051.
27. M. Vogelsberger and S. D. M. White, *Mon. Not. R. Astron. Soc.* **413**, 1419 (2011), doi:10.1111/j.1365-2966.2011.18224.x.
28. A. Vaquero, J. Redondo and J. Stadler, *J. Cosmol. Astropart. Phys.* **2019**, 012 (2019), arXiv:1809.09241 [astro-ph.CO], doi:10.1088/1475-7516/2019/04/012, [JCAP1904, no.04,012(2019)].
29. B. Eggemeier, J. Redondo, K. Dolag, J. C. Niemeyer and A. Vaquero, *Phys. Rev. Lett.* **125**, 041301 (2020), arXiv:1911.09417 [astro-ph.CO], doi:10.1103/physrevlett.125.041301.
30. P. Tinyakov, I. Tkachev and K. Zioutas, *J. Cosmol. Astropart. Phys.* **2016**, 035 (2016), doi:10.1088/1475-7516/2016/01/035.
31. V. I. Dokuchaev, Y. N. Eroshenko and I. I. Tkachev, *J. Exp. Theor. Phys.* **125**, 434 (2017), arXiv:1710.09586 [astro-ph.GA], doi:10.1134/s1063776117080039.
32. N. W. Evans, C. A. J. O’Hare and C. McCabe, *Phys. Rev. D* **99**, 023012 (2019), doi:10.1103/PhysRevD.99.023012.
33. V. Belokurov, D. B. Zucker, N. W. Evans, G. Gilmore, S. Vidrih, D. M. Bramich, H. J. Newberg, R. F. G. Wyse, M. J. Irwin, M. Fellhauer, P. C. Hewett, N. A. Walton, M. I. Wilkinson, N. Cole, B. Yanny, C. M. Rockosi, T. C. Beers, E. F. Bell, J. Brinkmann, Z. Ivezić and R. Lupton, *Astrophys. J.* **642**, L137 (2006), doi:10.1086/504797.
34. A. Helmi, *Annu. Rev. Astron. Astrophys.* **58**, 205 (2020), doi:10.1146/annurev-astro-032620-021917.

35. R. P. Naidu, C. Conroy, A. Bonaca, B. D. Johnson, Y.-S. Ting, N. Caldwell, D. Zaritsky and P. A. Cargile, *Astrophys. J.* **901**, 48 (2020), doi:10.3847/1538-4357/abaef4.
36. G. C. Myeong, N. W. Evans, V. Belokurov, J. L. Sanders and S. E. Kuposov, *Mon. Not. R. Astron. Soc.* **478**, 5449 (2018), <https://academic.oup.com/mnras/article-pdf/478/4/5449/25105825/sty1403.pdf>, doi:10.1093/mnras/sty1403.
37. G. C. Myeong, E. Vasiliev, G. Iorio, N. W. Evans and V. Belokurov, *Mon. Not. R. Astron. Soc.* **488**, 1235 (2019), doi:10.1093/mnras/stz1770.
38. H. H. Koppelman, A. Helmi, D. Massari, S. Roelenga and U. Bastian, *Astron. Astrophys.* **625**, A5 (2019), doi:10.1051/0004-6361/201834769.
39. A. Helmi, C. Babusiaux, H. H. Koppelman, D. Massari, J. Veljanoski and A. G. A. Brown, *Nature* **563**, 85 (2018), doi:10.1038/s41586-018-0625-x.
40. V. Belokurov, D. Erkal, N. W. Evans, S. E. Kuposov and A. J. Deason, *Mon. Not. R. Astron. Soc.* **478**, 611 (2018), doi:10.1093/mnras/sty982.
41. G. Iorio and V. Belokurov, *Mon. Not. R. Astron. Soc.* **482**, 3868 (2018), doi:10.1093/mnras/sty2806.
42. A. J. Deason, V. Belokurov, S. E. Kuposov and L. Lancaster, *Astrophys. J.* **862**, L1 (2018), doi:10.3847/2041-8213/aad0ee.
43. R. P. Naidu, C. Conroy, A. Bonaca, D. Zaritsky, R. Weinberger, Y.-S. Ting, N. Caldwell, S. Tacchella, J. J. Han, J. S. Speagle and P. A. Cargile, *Astrophys. J.* **923**, 92 (2021), doi:10.3847/1538-4357/ac2d2d.
44. A. Arvanitaki, S. Dimopoulos, S. Dubovsky, N. Kaloper and J. March-Russell, *Phys. Rev. D* **81**, 123530 (2010), arXiv:0905.4720 [hep-th], doi:10.1103/PhysRevD.81.123530.
45. A. Arvanitaki and S. Dubovsky, *Phys. Rev. D* **83**, 044026 (2011), arXiv:1004.3558 [hep-th], doi:10.1103/PhysRevD.83.044026.
46. A. Arvanitaki, M. Baryakhtar and X. Huang, *Phys. Rev. D* **91**, 084011 (2015), arXiv:1411.2263 [hep-ph], doi:10.1103/PhysRevD.91.084011.
47. R. Brito, V. Cardoso and P. Pani, *Class. Quantum Grav.* **32**, 134001 (2015), arXiv:1411.0686 [gr-qc], doi:10.1088/0264-9381/32/13/134001.
48. R. Brito, V. Cardoso and P. Pani, *Superradiance, Lecture Notes in Physics*, Vol. 906 (Springer, Cham, 2015), arXiv:1501.06570 [gr-qc], doi:10.1007/978-3-319-19000-6.
49. A. Arvanitaki, M. Baryakhtar, S. Dimopoulos, S. Dubovsky and R. Lasenby, *Phys. Rev. D* **95**, 043001 (2017), arXiv:1604.03958 [hep-ph], doi:10.1103/PhysRevD.95.043001.
50. D. J. E. Marsh, *Phys. Rep.* **643**, 1 (2016), arXiv:1510.07633 [astro-ph.CO], doi:10.1016/j.physrep.2016.06.005.
51. H. Yoshino and H. Kodama, *Prog. Theor. Exp. Phys.* **2014**, 043E02 (2014), arXiv:1312.2326 [gr-qc], doi:10.1093/ptep/ptu029.
52. S. D'Antonio *et al.*, *Phys. Rev. D* **98**, 103017 (2018), arXiv:1809.07202 [gr-qc], doi:10.1103/PhysRevD.98.103017.
53. L. Tsukada, T. Callister, A. Matas and P. Meyers, *Phys. Rev. D* **99**, 103015 (2019), arXiv:1812.09622 [astro-ph.HE], doi:10.1103/PhysRevD.99.103015.
54. S. J. Zhu, M. Baryakhtar, M. A. Papa, D. Tsuna, N. Kawanaka and H.-B. Eggenstein, *Phys. Rev. D* **102**, 063020 (2020), arXiv:2003.03359 [gr-qc], doi:10.1103/PhysRevD.102.063020.
55. KAGRA, VIRGO, LIGO Scientific Collab. (R. Abbott *et al.*), *Phys. Rev. D* **105**, 102001 (2022), arXiv:2111.15507 [astro-ph.HE], doi:10.1103/PhysRevD.105.102001.
56. H. Yoshino and H. Kodama, *Class. Quantum Grav.* **32**, 214001 (2015), arXiv:1505.00714 [gr-qc], doi:10.1088/0264-9381/32/21/214001.
57. A. Gruzinov, Black hole spindown by light bosons, arXiv:1604.06422 [astro-ph.HE] (2016).
58. M. Baryakhtar, M. Galanis, R. Lasenby and O. Simon, *Phys. Rev. D* **103**, 095019 (2021), arXiv:2011.11646 [hep-ph], doi:10.1103/PhysRevD.103.095019.

59. H. Omiya, T. Takahashi, T. Tanaka and H. Yoshino, *J. Cosmol. Astropart. Phys.* **2023**, 016 (2022).
60. P. Sikivie, *Phys. Rev. Lett.* **51**, 1415 (1983), doi:10.1103/PhysRevLett.51.1415 [Erratum-ibid **52**, 695 (1984)].
61. R. Barbieri, M. Cerdonio, G. Fiorentini and S. Vitale, *Phys. Lett. B* **226**, 357 (1989).
62. R. Barbieri, C. Braggio, G. Carugno, C. Gallo, A. Lombardi, A. Ortolan, R. Pengo, G. Ruoso and C. Speake, *Phys. Dark Univ.* **15**, 135 (2017).
63. N. Crescini, C. Braggio, G. Carugno, A. Ortolan and G. Ruoso, *Appl. Phys. Lett.* **117**, 144001 (2020).
64. N. Crescini, C. Braggio, G. Carugno, R. Di Vora, A. Ortolan and G. Ruoso, *Commun. Phys.* **3**, 164 (2020).
65. N. Crescini, C. Braggio, G. Carugno, A. Ortolan and G. Ruoso, *Phys. Rev. B* **104**, 064426 (2021), doi:10.1103/PhysRevB.104.064426.
66. QUAX Collab. (N. Crescini, D. Alesini, C. Braggio, G. Carugno, D. D'Agostino, D. Di Gioacchino, P. Falferi, U. Gambardella, C. Gatti, G. Iannone, C. Ligi, A. Lombardi, A. Ortolan, R. Pengo, G. Ruoso and L. Taffarello), *Phys. Rev. Lett.* **124**, 171801 (2020), arXiv:2001.08940 [hep-ex], doi:10.1103/PhysRevLett.124.171801.
67. D. Alesini, C. Braggio, G. Carugno, N. Crescini, D. D'Agostino, D. Di Gioacchino, R. Di Vora, P. Falferi, U. Gambardella, C. Gatti, G. Iannone, C. Ligi, A. Lombardi, G. Maccarrone, A. Ortolan, R. Pengo, C. Pira, A. Rettaroli, G. Ruoso, L. Taffarello and S. Tocci, *Nucl. Instrum. Methods A* **985**, 164641 (2021).
68. D. Alesini, C. Braggio, G. Carugno, N. Crescini, D. D'Agostino, D. Di Gioacchino, R. Di Vora, P. Falferi, S. Gallo, U. Gambardella, C. Gatti, G. Iannone, G. Lamanna, C. Ligi, A. Lombardi, R. Mezzena, A. Ortolan, R. Pengo, N. Pompeo, A. Rettaroli, G. Ruoso, E. Silva, C. C. Speake, L. Taffarello and S. Tocci, *Phys. Rev. D* **99**, 101101 (2019), arXiv:1903.06547 [physics.ins-det], doi:10.1103/PhysRevD.99.101101.
69. D. Di Gioacchino, C. Gatti, D. Alesini, C. Ligi, S. Tocci, A. Rettaroli, G. Carugno, N. Crescini, G. Ruoso, C. Braggio, P. Falferi, C. S. Gallo, U. Gambardella, G. Iannone, N. Lamanna, A. Lombardi, R. Mezzena, A. Ortolan, R. Pengo, E. Silva and N. Pompeo, *IEEE Trans. Appl. Superconduct.* **29**, 1 (2019), doi:10.1109/TASC.2019.2897267.
70. ADMX Collab. (T. Braine, R. Cervantes, N. Crisosto, N. Du, S. Kimes, L. J. Rosenberg, G. Rybka, J. Yang, D. Bowering, A. S. Chou, R. Khatiwada, A. Sonnenschein, W. Wester, G. Carosi, N. Woollett, L. D. Duffy, R. Bradley, C. Boutan, M. Jones, B. H. LaRoque, N. S. Oblath, M. S. Taubman, J. Clarke, A. Dove, A. Eddins, S. R. O'Kelley, S. Nawaz, I. Siddiqi, N. Stevenson, A. Agrawal, A. V. Dixit, J. R. Gleason, S. Jois, P. Sikivie, J. A. Solomon, N. S. Sullivan, D. B. Tanner, E. Lentz, E. J. Daw, J. H. Buckley, P. M. Harrington, E. A. Henriksen and K. W. Murch), *Phys. Rev. Lett.* **124**, 101303 (2020), arXiv:1910.08638 [hep-ex], doi:10.1103/PhysRevLett.124.101303.
71. R. D. Peccei and H. R. Quinn, *Phys. Rev. Lett.* **38**, 1440 (1977), doi:10.1103/PhysRevLett.38.1440.
72. J. Preskill, M. B. Wise and F. Wilczek, *Phys. Lett. B* **120**, 127 (1983), doi:http://dx.doi.org/10.1016/0370-2693(83)90637-8.
73. P. Svrcek and E. Witten, *J. High Energy Phys.* **6**, 051 (2006), hep-th/0605206, doi:10.1088/1126-6708/2006/06/051.
74. L. Di Luzio, A. Ringwald and C. Tamarit, *Phys. Rev. D* **98**, 095011 (2018), doi:10.1103/PhysRevD.98.095011.
75. R. T. Co, F. D'Eramo and L. J. Hall, *Phys. Rev. D* **94**, 075001 (2016), doi:10.1103/PhysRevD.94.075001.
76. Y. Kahn, B. R. Safdi and J. Thaler, *Phys. Rev. Lett.* **117**, 141801 (2016), doi:10.1103/PhysRevLett.117.141801.

77. S. Chaudhuri, K. Irwin, P. Graham and J. Mardon, arXiv:1904.05806 [hep-ex] (2019).
78. J. Yang, J. R. Gleason, S. Jois, I. Stern, P. Sikivie, N. S. Sullivan and D. B. Tanner, *Springer Proc. Phys.* **245**, 53 (2020), doi:10.1007/978-3-030-43761-9_7.
79. F. Wilczek, *Phys. Rev. Lett.* **40**, 279 (1978), doi:10.1103/PhysRevLett.40.279.
80. R. D. Peccei and H. R. Quinn, *Phys. Rev. D* **16**, 1791 (1977), doi:10.1103/PhysRevD.16.1791.
81. S. Weinberg, *Phys. Rev. Lett.* **40**, 223 (1978), doi:10.1103/PhysRevLett.40.223.
82. J. L. Ouellet, C. P. Salemi, J. W. Foster, R. Henning, Z. Bogorad, J. M. Conrad, J. A. Formaggio, Y. Kahn, J. Minervini, A. Radovinsky, N. L. Rodd, B. R. Safdi, J. Thaler, D. Winklehner and L. Winslow, *Phys. Rev. Lett.* **122**, 121802 (2019), arXiv:1810.12257 [hep-ex], doi:10.1103/PhysRevLett.122.121802.
83. A. V. Gramolin, D. Aybas, D. Johnson, J. Adam and A. O. Sushkov, *Nat. Phys.* **17**, 79 (2020), doi:10.1038/s41567-020-1006-6.
84. C. P. Salemi, J. W. Foster, J. L. Ouellet, A. Gavin, K. M. W. Pappas, S. Cheng, K. A. Richardson, R. Henning, Y. Kahn, R. Nguyen, N. L. Rodd, B. R. Safdi and L. Winslow, *Phys. Rev. Lett.* **127**, 081801 (2021), doi:10.1103/PhysRevLett.127.081801.
85. N. Crisosto, P. Sikivie, N. S. Sullivan, D. B. Tanner, J. Yang and G. Rybka, *Phys. Rev. Lett.* **124**, 241101 (2020), doi:10.1103/PhysRevLett.124.241101.
86. S. Lee, S. Ahn, J. Choi, B. R. Ko and Y. K. Semertzidis, *Phys. Rev. Lett.* **124**, 101802 (2020), arXiv:2001.05102 [hep-ex], doi:10.1103/PhysRevLett.124.101802.
87. O. Kwon, D. Lee, W. Chung, D. Ahn, H. Byun, F. Caspers, H. Choi, J. Choi, Y. Chong, H. Jeong, J. Jeong, J. E. Kim, J. Kim, I. M. C. B. U. Kutlu, J. Lee, M. Lee, S. Lee, A. Matlashov, S. Oh, S. Park, S. Uchaikin, S. Youn and Y. K. Semertzidis, *Phys. Rev. Lett.* **126**, 191802 (2021), doi:10.1103/PhysRevLett.126.191802.
88. M. Dine, W. Fischler and M. Srednicki, *Phys. Lett. B* **104**, 199 (1981), doi:10.1016/0370-2693(81)90590-6.
89. Ç. Kutlu, A. F. van Loo, S. V. Uchaikin, A. N. Matlashov, D. Lee, S. Oh, J. Kim, W. Chung, Y. Nakamura and Y. K. Semertzidis, *Superconduct. Sci. Technol.* **34**, 085013 (2021), doi:10.1088/1361-6668/abf23b.
90. D. Kim, J. Jeong, S. Youn, Y. Kim and Y. K. Semertzidis, *J. Cosmol. Astropart. Phys.* **2020**, 066 (2020), doi:10.1088/1475-7516/2020/03/066.
91. J. Jeong, S. Youn, S. Ahn, C. Kang and Y. K. Semertzidis, *Astropart. Phys.* **97**, 33 (2018), doi:https://doi.org/10.1016/j.astropartphys.2017.10.012.
92. D. Ahn, O. Kwon, W. Chung, W. Jang, D. Lee, J. Lee, S. W. Youn, D. Youm and Y. K. Semertzidis, Superconducting cavity in a high magnetic field, arXiv:2002.08769 (2020).
93. J. Jeong, S. Youn, S. Ahn, J. E. Kim and Y. K. Semertzidis, *Phys. Lett. B* **777**, 412 (2018), doi:https://doi.org/10.1016/j.physletb.2017.12.066.
94. B. Majorovits and for the MADMAX interest group, *J. Phys.: Conf. Ser.* **1342**, 012098 (2020).
95. D. Budker, P. W. Graham, M. Ledbetter, S. Rajendran and A. O. Sushkov, *Phys. Rev. X* **4**, 021030 (2014), arXiv:1306.6089 [hep-ph], doi:10.1103/PhysRevX.4.021030.
96. G. Ballesteros, J. Redondo, A. Ringwald and C. Tamarit, *J. Cosmol. Astropart. Phys.* **2017**, 001 (2017), doi:10.1088/1475-7516/2017/08/001.
97. B. T. Mcallister, S. R. Parker, E. N. Ivanov and M. E. Tobar, *IEEE Trans. Ultrason., Ferroelectr., Freq. Control* **66**, 236 (2019), doi:10.1109/TUFFC.2018.2881754.
98. D. Ahn, D. Youm, O. Kwon, W. Chung and Y. K. Semertzidis, High quality factor high-temperature superconducting microwave cavity development for the dark matter axion search in a strong magnetic field, arXiv:1902.04551 [physics.ins-det] (2019).

99. G. Flower, B. McAllister, M. Goryachev and M. E. Tobar, *Appl. Phys. Lett.* **117**, 162401 (2020), <https://doi.org/10.1063/5.0023547>, doi:10.1063/5.0023547.
100. L. S. Kuzmin, A. S. Sobolev, C. Gatti, D. Di Gioacchino, N. Crescini, A. Gordeeva and E. Il'ichev, *IEEE Trans. Appl. Supercond.* **28**, 1 (2018), doi:10.1109/TASC.2018.2850019.
101. M. Goryachev, B. T. McAllister and M. E. Tobar, *Phys. Dark Univ.* **26**, 100345 (2019), doi:<https://doi.org/10.1016/j.dark.2019.100345>.
102. C. A. Thomson, B. T. McAllister, M. Goryachev, E. N. Ivanov and M. E. Tobar, *Phys. Rev. Lett.* **126**, 081803 (2021), doi:10.1103/PhysRevLett.126.081803.
103. P. Sikivie, Superconducting radio frequency cavities as axion dark matter detectors, arXiv:1009.0762 [hep-ph] (2013).
104. R. Lasenby, *Phys. Rev. D* **102**, 015008 (2020), doi:10.1103/PhysRevD.102.015008.
105. A. Berlin, R. T. D'Agnolo, S. A. R. Ellis, C. Nantista, J. Neilson, P. Schuster, S. Tantawi, N. Toro and K. Zhou, *J. High Energy Phys.* **2020**, 88 (2020), doi:10.1007/JHEP07(2020)088.
106. J. P. Turneaure, C. M. Will, B. F. Farrell, E. M. Mattison and R. F. C. Vessot, *Phys. Rev. D* **27**, 1705 (1983), doi:10.1103/PhysRevD.27.1705.
107. M. E. Tobar, P. Wolf, S. Bize, G. Santarelli and V. Flambaum, *Phys. Rev. D* **81**, 022003 (2010), doi:10.1103/PhysRevD.81.022003.
108. M. Goryachev, Z. Kuang, E. N. Ivanov, P. Haslinger, H. Müller and M. E. Tobar, *IEEE Trans. Ultrason., Ferroelectr., Freq. Control* **65**, 991 (2018), doi:10.1109/TUFFC.2018.2824845.
109. M. E. Tobar, P. L. Stanwix, J. J. McFerran, J. Guéna, M. Abgrall, S. Bize, A. Clairon, P. Laurent, P. Rosenbusch, D. Rovera and G. Santarelli, *Phys. Rev. D* **87**, 122004 (2013), doi:10.1103/PhysRevD.87.122004.
110. M. Nagel et al., *Nat. Commun.* **6**, 8174 (2015).
111. E. N. Ivanov and M. E. Tobar, *IEEE Trans. Ultrason., Ferroelectr., Freq. Control* **56**, 263 (2009), doi:10.1109/TUFFC.2009.1035.
112. E. Ivanov, M. Tobar and R. Woode, *IEEE Trans. Ultrason., Ferroelectr., Freq. Control* **45**, 1526 (1998).
113. J. Bourhill, E. Ivanov and M. E. Tobar, *Phys. Rev. A* **92**, 023817 (2015), doi:10.1103/PhysRevA.92.023817.
114. P. A. Bushev, J. Bourhill, M. Goryachev, N. Kukharchyk, E. Ivanov, S. Galliou, M. E. Tobar and S. Danilishin, *Phys. Rev. D* **100**, 066020 (2019), doi:10.1103/PhysRevD.100.066020.
115. E. N. Ivanov and M. E. Tobar, Generation of spectrally pure microwave signals, arXiv:2003.09117 [physics.ins-det] (2020).
116. M. E. Tobar, P. Wolf, S. Bize, G. Santarelli and V. Flambaum, *Phys. Rev. D* **81**, 022003 (2010), doi:10.1103/PhysRevD.81.022003.
117. A. Lo, P. Haslinger, E. Mizrachi, L. Anderegg, H. Müller, M. Hohensee, M. Goryachev and M. E. Tobar, *Phys. Rev. X* **6**, 011018 (2016), doi:10.1103/PhysRevX.6.011018.
118. R. E. Desrochers, M. Koehnke and J. Searls, *Raytheon Technol. Today* **1**, 42.
119. M. E. Tobar, B. T. McAllister and M. Goryachev, *Phys. Dark Univ.* **26**, 100339 (2019), doi:<https://doi.org/10.1016/j.dark.2019.100339>.
120. M. E. Tobar, B. T. McAllister and M. Goryachev, *Phys. Dark Univ.* **30**, 100624 (2020), doi:<https://doi.org/10.1016/j.dark.2020.100624>.
121. B. T. McAllister, M. Goryachev, J. Bourhill, E. N. Ivanov and M. E. Tobar, Broadband axion dark matter haloscopes via electric sensing, arXiv:1803.07755 [physics.ins-det] (2018).
122. J. Ouellet and Z. Bogorad, *Phys. Rev. D* **99**, 055010 (2019), doi:10.1103/PhysRevD.99.055010.

123. M. Beutter, A. Pargner, T. Schwetz and E. Todarello, *J. Cosmol. Astropart. Phys.* **2019**, 026 (2019), doi:10.1088/1475-7516/2019/02/026.
124. Y. Kim, D. Kim, J. Jeong, J. Kim, Y. C. Shin and Y. K. Semertzidis, *Phys. Dark Univ.* **26**, 100362 (2019), doi:https://doi.org/10.1016/j.dark.2019.100362.
125. P. W. Graham and S. Rajendran, *Phys. Rev. D* **84**, 055013 (2011), doi:10.1103/PhysRevD.84.055013.
126. T. Wu, J. W. Blanchard, G. P. Centers, N. L. Figueroa, A. Garcon, P. W. Graham, D. F. J. Kimball, S. Rajendran, Y. V. Stadnik, A. O. Sushkov, A. Wickenbrock and D. Budker, *Phys. Rev. Lett.* **122**, 191302 (2019), doi:10.1103/PhysRevLett.122.191302.
127. C. Abel *et al.*, *Phys. Rev. X* **7**, 041034 (2017), doi:10.1103/PhysRevX.7.041034.
128. C. Balanis, *Advanced Engineering Electromagnetics*, 2nd edn. (Wiley, 2012).
129. R. Harrington, *Introduction to Electromagnetic Engineering*, Dover Books on Electrical Engineering Series (Dover Publications, Mineola, NY, 2003).
130. M. E. Tobar, B. T. McAllister and M. Goryachev, *Phys. Rev. Appl.* **15**, 014007 (2021), doi:10.1103/PhysRevApplied.15.014007.
131. R. Becker and F. Sauter, *Electromagnetic Fields and Interactions, Blaisdell Book in the pure and Applied Sciences*, No. 1-2 (Dover Publications, 1982).
132. P. Kinsler, A. Favaro and M. W. McCall, *Eur. J. Phys.* **30**, 983 (2009), doi:10.1088/0143-0807/30/5/007.
133. R. N. C. Pfeifer, T. A. Nieminen, N. R. Heckenberg and H. Rubinsztein-Dunlop, *Rev. Mod. Phys.* **79**, 1197 (2007), doi:10.1103/RevModPhys.79.1197.
134. J. E. Kim, *Phys. Rev. Lett.* **43**, 103 (1979), doi:10.1103/PhysRevLett.43.103.
135. J. Jeong, S. Youn, S. Bae, J. Kim, T. Seong, J. E. Kim and Y. K. Semertzidis, *Phys. Rev. Lett.* **125**, 221302 (2020), doi:10.1103/PhysRevLett.125.221302.
136. B. T. McAllister, G. Flower, E. N. Ivanov, M. Goryachev, J. Bourhill and M. E. Tobar, *Phys. Dark Univ.* **18**, 67 (2017), arXiv:1706.00209 [physics.ins-det], doi:10.1016/j.dark.2017.09.010.
137. A. P. Quiskamp, B. T. McAllister, G. Rybka and M. E. Tobar, *Phys. Rev. Appl.* **14**, 044051 (2020), arXiv:2006.05641 [physics.ins-det], doi:10.1103/PhysRevApplied.14.044051.
138. P. W. Graham and S. Rajendran, *Phys. Rev. D* **88**, 035023 (2013), arXiv:1306.6088 [hep-ph], doi:10.1103/PhysRevD.88.035023.
139. J. Jaeckel and A. Ringwald, *Annu. Rev. Nucl. Part. Sci.* **60**, 405 (2010), arXiv:1002.0329 [hep-ph], doi:10.1146/annurev.nucl.012809.104433.
140. S. Borsanyi *et al.*, Lattice QCD for cosmology, arXiv:1606.07494 (2016).
141. B. M. Brubaker, L. Zhong, Y. V. Gurevich, S. B. Cahn, S. K. Lamoreaux, M. Simanovskaia, J. R. Root, S. M. Lewis, S. Al Kenany, K. M. Backes, I. Urdinaran, N. M. Rapidis, T. M. Shokair, K. A. van Bibber, D. A. Palken, M. Malnou, W. F. Kindel, M. A. Anil, K. W. Lehnert and G. Carosi, *Phys. Rev. Lett.* **118**, 061302 (2017), arXiv:1610.02580 [astro-ph.CO], doi:10.1103/PhysRevLett.118.061302.
142. MADMAX Working Group Collab. (A. Caldwell, G. Dvali, B. Majorovits, A. Millar, G. Raffelt, J. Redondo, O. Reimann, F. Simon and F. Steffen), *Phys. Rev. Lett.* **118**, 091801 (2017), arXiv:1611.05865 [physics.ins-det], doi:10.1103/PhysRevLett.118.091801.
143. A. J. Millar, J. Redondo and F. D. Steffen, *J. Cosmol. Astropart. Phys.* **2017**, 006 (2017), doi:10.1088/1475-7516/2017/10/006.
144. MADMAX Collab. (P. Brun *et al.*), *Eur. Phys. J. C* **79**, 186 (2019), arXiv:1901.07401 [physics.ins-det], doi:10.1140/epjc/s10052-019-6683-x.
145. G. Carosi, G. Rybka and K. van Bibber, *Microwave Cavities and Detectors for Axion Research*, Springer Proceedings in Physics (Springer, 2017).
146. J. L. Doane, *Int. J. Infrared Millimeter Waves* **5**, 737 (1984), doi:10.1007/BF01009605.

147. M. Morpurgo, *Cryogenics* **19**, 411 (1979), doi:[https://doi.org/10.1016/0011-2275\(79\)90126-7](https://doi.org/10.1016/0011-2275(79)90126-7).
148. The MADMAX Collab. (C. Lee, X. LiJ, D. Strom and O. Reimann), *J. Phys.: Conf. Series* **2156**, 012041 (2021), doi:[10.1088/1742-6596/2156/1/012041](https://doi.org/10.1088/1742-6596/2156/1/012041).
149. S. Borsanyi, Z. Fodor, J. Guenther, K.-H. Kampert, S. D. Katz, T. Kawanai, T. G. Kovacs, S. W. Mages, A. Pasztor, F. Pittler, J. Redondo, A. Ringwald and K. K. Szabo, *Nature* **539**, 69 (2016), arXiv:1606.07494 [hep-lat], doi:[10.1038/nature20115](https://doi.org/10.1038/nature20115).
150. ADMX Collab. (N. Du, N. Force, R. Khatiwada, E. Lentz, R. Ottens, L. J. Rosenberg, G. Rybka, G. Carosi, N. Woollett, D. Bowring, A. S. Chou, A. Sonnenschein, W. Wester, C. Boutan, N. S. Oblath, R. Bradley, E. J. Daw, A. V. Dixit, J. Clarke, S. R. O'Kelley, N. Crisosto, J. R. Gleason, S. Jois, P. Sikivie, I. Stern, N. S. Sullivan, D. B. Tanner and G. C. Hilton), *Phys. Rev. Lett.* **120**, 151301 (2018), arXiv:1804.05750 [hep-ex], doi:[10.1103/PhysRevLett.120.151301](https://doi.org/10.1103/PhysRevLett.120.151301).
151. D. E. Morris, An electromagnetic detector for relic axions, Technical Report, Report No. LBL-17915 (1984).
152. D. Antypas, O. Tretiak, K. Zhang, A. Garcon, G. Perez, M. G. Kozlov, S. Schiller and D. Budker, *Quantum Sci. Technol.* **6**, 034001 (2021), doi:[10.1088/2058-9565/abe472](https://doi.org/10.1088/2058-9565/abe472).
153. M. Jiang, H. Su, Z. Wu, X. Peng and D. Budker, *Sci. Adv.* **7**, eabe0719 (2021), <https://www.science.org/doi/pdf/10.1126/sciadv.abe0719>, doi:[10.1126/sciadv.abe0719](https://doi.org/10.1126/sciadv.abe0719).
154. W. Wuensch, S. De Panfilis-Wuensch, Y. K. Semertzidis, J. T. Rogers, A. C. Melissinos, H. J. Halama, B. E. Moskowitz, A. G. Prodell, W. B. Fowler and F. A. Nezrick, *Phys. Rev. D* **40**, 3153 (1989), doi:[10.1103/PhysRevD.40.3153](https://doi.org/10.1103/PhysRevD.40.3153).
155. S. Moriyama et al., *Phys. Lett. B* **434**, 147 (1998), arXiv:hep-ex/9805026 [hep-ex], doi:[10.1016/S0370-2693\(98\)00766-7](https://doi.org/10.1016/S0370-2693(98)00766-7).
156. V. Anastassopoulos et al., *Nat. Phys.* **13**, 584 (2017), arXiv:1705.02290 [hep-ex], doi:[10.1038/nphys4109](https://doi.org/10.1038/nphys4109).
157. CAST Collab. (S. Andriamonje et al.), *J. Cosmol. Astropart. Phys.* **704**, 010 (2007), arXiv:hep-ex/0702006.
158. CAST Collab. (E. Arik et al.), *J. Cosmol. Astropart. Phys.* **902**, 008 (2009), arXiv:0810.4482 [hep-ex], doi:[10.1088/1475-7516/2009/02/008](https://doi.org/10.1088/1475-7516/2009/02/008).
159. I. G. Irastorza, F. Avignone, S. Caspi, J. Carmona, T. Dafni et al., *J. Cosmol. Astropart. Phys.* **1106**, 13 (2011), arXiv:1103.5334 [hep-ex], doi:[10.1088/1475-7516/2011/06/013](https://doi.org/10.1088/1475-7516/2011/06/013).
160. IAXO Collab. (E. Armengaud et al.), *J. Cosmol. Astropart. Phys.* **6**, 047 (2019), arXiv:1904.09155 [hep-ph], doi:[10.1088/1475-7516/2019/06/047](https://doi.org/10.1088/1475-7516/2019/06/047).
161. IAXO Collab. (A. Abeln et al.), *J. High Energy Phys.* **5**, 137 (2021), arXiv:2010.12076 [physics.ins-det], doi:[10.1007/JHEP05\(2021\)137](https://doi.org/10.1007/JHEP05(2021)137).
162. R. Shah, K.-S. Isleif, F. Januschek, A. Lindner and M. Schott, TES detector for ALPS II, in *Proc. European Physical Society Conf. High Energy Physics — PoS(EPS-HEP2021)* (2022), p. 801.
163. A. Hallal, G. Messineo, M. D. Ortiz, J. Gleason, H. Hollis, D. Tanner, G. Mueller and A. Spector, *Phys. Dark Univ.* **1**, 100914 (2021), doi:<https://doi.org/10.1016/j.dark.2021.100914>.
164. M. D. Ortiz, J. Gleason, H. Grote, A. Hallal, M. Hartman, H. Hollis, K.-S. Isleif, A. James, K. Karan, T. Kozłowski et al., *Phys. Dark Univ.* **35**, 100968 (2022).
165. A. G. Glenday, C. E. Cramer, D. F. Phillips and R. L. Walsworth, *Phys. Rev. Lett.* **101**, 261801 (2008), doi:[10.1103/PhysRevLett.101.261801](https://doi.org/10.1103/PhysRevLett.101.261801).
166. G. Vasilakis, J. M. Brown, T. W. Kornack and M. V. Romalis, *Phys. Rev. Lett.* **103**, 261801 (2009), arXiv:0809.4700 [physics.atom-ph], doi:[10.1103/PhysRevLett.103.261801](https://doi.org/10.1103/PhysRevLett.103.261801).

167. D. J. Wineland, J. J. Bollinger, D. J. Heinzen, W. M. Itano and M. G. Raizen, *Phys. Rev. Lett.* **67**, 1735 (1991), doi:10.1103/PhysRevLett.67.1735.
168. J. E. Moody and F. Wilczek, *Phys. Rev. D* **30**, 130 (1984), doi:10.1103/PhysRevD.30.130.
169. P.-H. Chu, A. Dennis, C. B. Fu, H. Gao, R. Khatiwada, G. Laskaris, K. Li, E. Smith, W. M. Snow, H. Yan and W. Zheng, *Phys. Rev. D* **87**, 011105 (2013), doi:10.1103/PhysRevD.87.011105.
170. M. Bulatowicz, R. Griffith, M. Larsen, J. Mirijanian, C. B. Fu, E. Smith, W. M. Snow, H. Yan and T. G. Walker, *Phys. Rev. Lett.* **111**, 102001 (2013), doi:10.1103/PhysRevLett.111.102001.
171. J. Lee, A. Almasi and M. Romalis, *Phys. Rev. Lett.* **120**, 161801 (2018), doi:10.1103/PhysRevLett.120.161801.
172. H. Fosbinder-Elkins, C. Lohmeyer, J. Dargert, M. Cunningham, M. Harkness, E. Levenson-Falk, S. Mumford, A. Kapitulnik, A. Arvanitaki, I. Lee, E. Smith, E. Wiesman, J. Shortino, J. C. Long, W. M. Snow, C.-Y. Liu, Y. Shin, Y. Semertzidis and Y.-H. Lee, Progress on the ariadne axion experiment, in *Microwave Cavities and Detectors for Axion Research*, eds. G. Carosi, G. Rybka and K. van Bibber (Springer International Publishing, Cham, 2018), pp. 151–161.
173. G. Raffelt, *Phys. Rev. D* **86**, 15001 (2012), arXiv:1205.1776 [hep-ph], doi:10.1103/PhysRevD.86.015001.
174. M. Jiang, H. Su, A. Garcon, X. Peng and D. Budker, *Nat. Phys.* **17**, 1402 (2021), doi:10.1038/s41567-021-01392-z.
175. M. Batz, P. J. Nacher and G. Tastevin, *J. Phys.: Conf. Series* **294**, 12002 (2011), doi:10.1088/1742-6596/294/1/012002.
176. A. N. Youdin, J. Krause, D. K. Jagannathan, L. R. Hunter and S. K. Lamoreaux, *Phys. Rev. Lett.* **77**, 2170 (1996), doi:10.1103/PhysRevLett.77.2170.
177. A. Arvanitaki and A. A. Geraci, *Phys. Rev. Lett.* **113**, 161801 (2014), arXiv:1403.1290 [hep-ph], doi:10.1103/PhysRevLett.113.161801.
178. J. Schütte-Engel, D. J. E. Marsh, A. J. Millar, A. Sekine, F. Chadha-Day, S. Hoof, M. Ali, K.-C. Fong, E. Hardy and L. Šmejkal (2021), arXiv:2102.05366 [hep-ph].
179. C. M. Caves, *Phys. Rev. D* **26**, 1817 (1982), doi:10.1103/PhysRevD.26.1817.
180. B. R. Johnson, M. D. Reed, A. A. Houck, D. I. Schuster, L. S. Bishop, E. Ginossar, J. M. Gambetta, L. DiCarlo, L. Frunzio, S. M. Girvin and R. J. Schoelkopf, *Nat. Phys.* **6**, 663 (2010), 1003.2734, doi:10.1038/nphys1710.
181. S. Kono, K. Koshino, Y. Tabuchi, A. Noguchi and Y. Nakamura, *Nat. Phys.* **14**, 546 (2018), 1711.05479, doi:10.1038/s41567-018-0066-3.
182. M. Lawson, A. J. Millar, M. Pancaldi, E. Vitagliano and F. Wilczek, *Phys. Rev. Lett.* **123**, 141802 (2019), arXiv:1904.11872 [hep-ph], doi:10.1103/PhysRevLett.123.141802.
183. C. M. Caves, K. S. Thorne, R. W. P. Drever, V. D. Sandberg and M. Zimmermann, *Rev. Mod. Phys.* **52**, 341 (1980), doi:10.1103/RevModPhys.52.341.
184. E. Armengaud, F. T. Avignone, M. Betz, P. Brun, G. Cantatore, J. M. Carmona, G. P. Carosi, F. Caspers, S. Caspi *et al.*, *J. Instrum.* **9**, T05002 (2014), arXiv:1401.3233 [physics.ins-det], doi:10.1088/1748-0221/9/05/t05002.
185. ARIADNE Collab. (N. Aggarwal *et al.*), *Phys. Rev. Res.* **4**, 013090 (2022).
186. M. Silva-Feaver, S. Chaudhuri, H. Cho, C. Dawson, P. Graham, K. Irwin, S. Kuenstner, D. Li, J. Mardon, H. Moseley, R. Mule, A. Phipps, S. Rajendran, Z. Steffen and B. Young, *IEEE Trans. Appl. Supercond.* **27**, 1 (2017).
187. L. Zhong, S. Al Kenany, K. M. Backes, B. M. Brubaker, S. B. Cahn, G. Carosi, Y. V. Gurevich, W. F. Kindel, S. K. Lamoreaux, K. W. Lehnert, S. M. Lewis, M. Malnou, R. H. Maruyama, D. A. Palken, N. M. Rapidis, J. R. Root, M. Simanovskaia, T. M.

- Shokair, D. H. Speller, I. Urdinaran and K. A. van Bibber, *Phys. Rev. D* **97**, 92001 (2018), arXiv:1803.03690 [hep-ex], doi:10.1103/PhysRevD.97.092001.
188. D. Horns, J. Jaeckel, A. Lindner, A. Lobanov, J. Redondo and A. Ringwald, *J. Cosmol. Astropart. Phys.* **4**, 016 (2013), arXiv:1212.2970 [hep-ph], doi:10.1088/1475-7516/2013/04/016.
189. Brass Website, <http://wwwiexp.desy.de/groups/astroparticle/brass/brassweb.htm> [accessed 6 July 2021].
190. BREAD Collab. (J. Liu et al.), *Phys. Rev. Lett.* **128**, 131801 (2022).
191. R. Gupta, M. Anerella, A. Ghosh, W. Sampson, J. Schmalzle, D. Konikowska, Y. K. Semertzidis and Y. Shin, *IEEE Trans. Appl. Superconduct.* **26**, 1 (2016), doi:10.1109/TASC.2016.2518240.
192. R. Gupta, M. Anerella, J. Cozzolino, P. Joshi, S. Joshi, S. Plate, W. Sampson, H. Song, P. Wanderer, W. Chung, J. Kim, B. R. Ko, S. W. Youn and Y. K. Semertzidis, *IEEE Trans. Appl. Superconduct.* **29**, 1 (2019), doi:10.1109/TASC.2019.2902319.
193. S. Hahn, K. Kim, K. Kim, X. Hu, T. Painter, I. Dixon, S. Kim, K. R. Bhattarai, S. Noguchi, J. Jaroszynski and D. C. Larbalestier, *Nature* **570**, 496 (2019), doi:10.1038/s41586-019-1293-1.
194. M. Malnou, D. Palken, B. Brubaker, L. R. Vale, G. C. Hilton and K. Lehnert, *Phys. Rev. X* **9**, 21023 (2019), arXiv:1809.06470 [quant-ph], doi:10.1103/PhysRevX.9.021023.
195. M. A. Shifman, A. I. Vainshtein and V. I. Zakharov, *Nucl. Phys. B* **166**, 493 (1980), doi:10.1016/0550-3213(80)90209-6.
196. B. M. Brubaker, L. Zhong, S. K. Lamoreaux, K. W. Lehnert and K. A. van Bibber, *Phys. Rev. D* **96**, 123008 (2017), doi:10.1103/PhysRevD.96.123008.
197. A. R. Zhitnitsky, *Sov. J. Nucl. Phys.* **31**, 260 (1980).
198. D. A. Palken, B. M. Brubaker, M. Malnou, S. A. Kenany, K. M. Backes, S. B. Cahn, Y. V. Gurevich, S. K. Lamoreaux, S. M. Lewis, R. H. Maruyama, N. M. Rapidis, J. R. Root, M. Simanovskaia, T. M. Shokair, S. Singh, D. H. Speller, I. Urdinaran, K. van Bibber, L. Zhong and K. W. Lehnert, *Phys. Rev. D* **101**, 123011 (2020), doi:10.1103/PhysRevD.101.123011.
199. M. Buschmann, J. W. Foster and B. R. Safdi, *Phys. Rev. Lett.* **124**, 161103 (2020), arXiv:1906.00967 [astro-ph.CO], doi:10.1103/PhysRevLett.124.161103.
200. A. V. Dixit, S. Chakram, K. He, A. Agrawal, R. K. Naik, D. I. Schuster and A. Chou, *Phys. Rev. Lett.* **126**, 141302 (2021), doi:10.1103/PhysRevLett.126.141302.
201. L. Di Luzio, M. Giannotti, E. Nardi and L. Visinelli, *Phys. Rep.* **870**, 1 (2020), doi: <https://doi.org/10.1016/j.physrep.2020.06.002>.
202. K. M. Backes, D. A. Palken, S. A. Kenany, B. M. Brubaker, S. B. Cahn, A. Droster, G. C. Hilton, S. Ghosh, H. Jackson, S. K. Lamoreaux, A. F. Leder, K. W. Lehnert, S. M. Lewis, M. Malnou, R. H. Maruyama, N. M. Rapidis, M. Simanovskaia, S. Singh, D. H. Speller, I. Urdinaran, L. R. Vale, E. C. van Assendelft, K. van Bibber and H. Wang, *Nature* **590**, 238 (2021), doi:10.1038/s41586-021-03226-7.
203. Y. Hochberg, I. Charaev, S.-W. Nam, V. Verma, M. Colangelo and K. K. Berggren, *Phys. Rev. Lett.* **123**, 151802 (2019), arXiv:1903.05101 [hep-ph], doi:10.1103/PhysRevLett.123.151802.
204. R. Li, J. Wang, X.-L. Qi and S.-C. Zhang, *Nat. Phys.* **6**, 284 (2010), arXiv:0908.1537 [cond-mat.other], doi:10.1038/nphys1534.
205. D. J. E. Marsh, K. C. Fong, E. W. Lentz, L. Šmejkal and M. N. Ali, *Phys. Rev. Lett.* **123**, 121601 (2019), arXiv:1807.08810 [hep-ph], doi:10.1103/PhysRevLett.123.121601.
206. J. Zhang, D. Wang, M. Shi, T. Zhu, H. Zhang and J. Wang, *Chin. Phys. Lett.* **37**, 077304 (2020), doi:10.1088/0256-307x/37/7/077304.

207. M. Malnou, D. A. Palken, L. R. Vale, G. C. Hilton and K. W. Lehnert, *Phys. Rev. Appl.* **9**, 044023 (2018), doi:10.1103/PhysRevApplied.9.044023.
208. T. Yamamoto, K. Inomata, M. Watanabe, K. Matsuba, T. Miyazaki, W. D. Oliver, Y. Nakamura and J. S. Tsai, *Appl. Phys. Lett.* **93**, 042510 (2008), doi:10.1063/1.2964182.
209. Particle Data Group Collab. (M. Tanabashi, K. Hagiwara, K. Hikasa, K. Nakamura, Y. Sumino, F. Takahashi, J. Tanaka, K. Agashe, G. Aielli, C. Amsler, M. Antonelli, D. M. Asner, H. Baer, S. Banerjee, R. M. Barnett, T. Basaglia, C. W. Bauer, J. J. Beatty, V. I. Belousov, J. Beringer, S. Bethke, A. Bettini, H. Bichsel, O. Biebel, K. M. Black, E. Blucher, O. Buchmuller, V. Burkert, M. A. Bychkov, R. N. Cahn, M. Carena, A. Ceccucci, A. Cerri, D. Chakraborty, M.-C. Chen, R. S. Chivukula, G. Cowan, O. Dahl, G. D'Ambrosio, T. Damour, D. de Florian, A. de Gouvêa, T. DeGrand, P. de Jong, G. Dissertori, B. A. Dobrescu, M. D'Onofrio, M. Doser, M. Drees, H. K. Dreiner, D. A. Dwyer, P. Eerola, S. Eidelman, J. Ellis, J. Erler, V. V. Ezhela, W. Fetscher, B. D. Fields, R. Firestone, B. Foster, A. Freitas, H. Gallagher, L. Garren, H.-J. Gerber, G. Gerbier, T. Gershon, Y. Gershtein, T. Gherghetta, A. A. Godizov, M. Goodman, C. Grab, A. V. Gribsan, C. Grojean, D. E. Groom, M. Grünewald, A. Gurtu, T. Gutsche, H. E. Haber, C. Hanhart, S. Hashimoto, Y. Hayato, K. G. Hayes, A. Hebecker, S. Heinemeyer, B. Heltsley, J. J. Hernández-Rey, J. Hisano, A. Höcker, J. Holder, A. Holtkamp, T. Hyodo, K. D. Irwin, K. F. Johnson, M. Kado, M. Karliner, U. F. Katz, S. R. Klein, E. Klempt, R. V. Kowalewski, F. Krauss, M. Kreps, B. Krusche, Y. V. Kuyanov, Y. Kwon, O. Lahav, J. Laiho, J. Lesgourgues, A. Liddle, Z. Ligeti, C.-J. Lin, C. Lippmann, T. M. Liss, L. Lit-tenberg, K. S. Lugovsky, S. B. Lugovsky, A. Lusiani, Y. Makida, F. Maltoni, T. Mannel, A. V. Manohar, W. J. Marciano, A. D. Martin, A. Masoni, J. Matthews, U.-G. Meißner, D. Milstead, R. E. Mitchell, K. Mönig, P. Molaro, F. Moortgat, M. Moskovic, H. Murayama, M. Narain, P. Nason, S. Navas, M. Neubert, P. Nevski, Y. Nir, K. A. Olive, S. Pagan Griso, J. Parsons, C. Patrignani, J. A. Peacock, M. Pennington, S. T. Petcov, V. A. Petrov, E. Pianori, A. Piepke, A. Pomarol, A. Quadt, J. Rademacker, G. Raffelt, B. N. Ratcliff, P. Richardson, A. Ringwald, S. Roesler, S. Rolli, A. Romaniouk, L. J. Rosenberg, J. L. Rosner, G. Rybka, R. A. Ryutin, C. T. Sachrajda, Y. Sakai, G. P. Salam, S. Sarkar, F. Sauli, O. Schneider, K. Scholberg, A. J. Schwartz, D. Scott, V. Sharma, S. R. Sharpe, T. Shutt, M. Silari, T. Sjöstrand, P. Skands, T. Skwarnicki, J. G. Smith, G. F. Smoot, S. Spanier, H. Spieler, C. Spiering, A. Stahl, S. L. Stone, T. Sumiyoshi, M. J. Syphers, K. Terashi, J. Terning, U. Thoma, R. S. Thorne, L. Tiator, M. Titov, N. P. Tkachenko, N. A. Törnqvist, D. R. Tovey, G. Valencia, R. Van de Water, N. Varelas, G. Venanzoni, L. Verde, M. G. Vincet, P. Vogel, A. Vogt, S. P. Wakely, W. Walkowiak, C. W. Walter, D. Wands, D. R. Ward, M. O. Wascko, G. Weiglein, D. H. Weinberg, E. J. Weinberg, M. White, L. R. Wiencke, S. Willocq, C. G. Wohl, J. Womersley, C. L. Woody, R. L. Workman, W.-M. Yao, G. P. Zeller, O. V. Zenin, R.-Y. Zhu, S.-L. Zhu, F. Zimmermann, P. A. Zyla, J. Anderson, L. Fuller, V. S. Lugovsky and P. Schaffner), *Phys. Rev. D* **98**, 030001 (2018), doi:10.1103/PhysRevD.98.030001.
210. A. Little, L. Wu, P. Lampen-Kelley, A. Banerjee, S. Patankar, D. Rees, C. A. Bridges, J. Q. Yan, D. Mandrus, S. E. Nagler and J. Orenstein, *Phys. Rev. Lett.* **119**, 227201 (2017), arXiv:1704.07357 [cond-mat.str-el], doi:10.1103/PhysRevLett.119.227201.